HELSINKI UNIVERSITY OF TECHNOLOGY

Faculty of Electronics, Communication and Automation

Heini Heikkilä

Measurement and control of the displacement of a magnetic shape memory actuator

Master's Thesis submitted in partial fulfillment of the requirements for the degree of Master of Science in Technology

20th October 2009

Supervisor: Professor Mervi Paulasto-Kröckel

Instructor: Juhani Tellinen, D.Sc.

HELSINKI UNIVERSITY OF TECHNOLOGY Abstract of the Master's Thesis

Author: Heini Heikkilä

Name of the thesis: Measurement and control of the displacement of a magnetic shape memory actuator

Number of pages: 67 Date: 21st August 2009

Faculty: Faculty of Electronics, Communication and Automation

Professorship: S-113 Electronics Production Technology

Supervisor: Professor Mervi Paulasto-Kröckel

Instructor: Juhani Tellinen, D.Sc.

Abstract text:

PURPOSE: The purpose of this thesis was to measure the fast displacement of a magnetic shape memory (MSM) actuator and to demonstrate the feedback control of the displacement.

MATERIALS AND METHODS: Ni-Mn-Ga is a magnetic shape memory alloy, which can produce large strains in magnetic field. In an actuator coils are used to generate the magnetic field and the strained MSM elements are compressed by a mechanical spring. The fast displacement of the actuator was measured using a laser sensor. A PID controller was implemented with LabVIEW and used in feedback control measurements. The performance of the controller in rapid displacements was tested and analyzed. The tuning of the controller was carried out experimentally. Additionally, the hysteresis of the actuator was measured and the current module that was used for driving the actuator was documented.

RESULTS: The displacement and hysteresis of the actuator were measured. The controller was successfully used to control the displacement, but also its weaknesses were shown and discussed. The measurements revealed problems in the stability of the MSM elements in actuator use. Accordingly, the measurements produced ideas for further development of the controller and for investigations of the microstructure of the MSM material.

CONCLUSIONS: The hysteresis of the MSM material and rapid displacements made the control challenging, but all in all the performance of the PID controller was either good or satisfactory. Implementation and optimization of an adaptive controller would solve several problems that arose during the measurements. However, improving the repeatability of the behavior of the MSM elements in actuator use is also important in order to obtain accurate control.

Key words: magnetic shape memory, MSM, PID control, feedback control, actuator

TEKNILLINEN KORKEAKOULU Diplomityön tiivistelmä

Tekijä: Heini Heikkilä

Työn nimi: Magneettisen muistimateriaaliaktuaattorin liikkeen mittaaminen ja ohjaus

Sivumäärä: 67 Päivämäärä: 21.8.2009

Tiedekunta: Elektroniikan, tietoliikenteen ja automaation tiedekunta

Professuuri: S-113 Elektroniikan valmistustekniikka

Työn valvoja: professori Mervi Paulasto-Kröckel

Työn ohjaaja: TkT Juhani Tellinen

Tiivistelmäteksti:

TYÖN TARKOITUS: Työn tarkoituksena oli mitata magneettisen muistimateriaali-aktuaattorin nopeaa liikettä sekä kehittää takaisinkytkentään perustuva liikkeen ohjaus.

MATERIAALIT JA MENETELMÄT: Ni-Mn-Ga on magneettinen muistimetalli, joka voi tuottaa liikettä magneettikentässä. Aktuaattorissa magneettikenttä saadaan aikaan keloilla, ja venynyt MSM-materiaali palautetaan jousen avulla alkuperäiseen pituuteensa. Työssä mitattiin aktuaattorin liike laseranturilla. Liikkeen nopeus ja hystereesi asettivat haasteita ohjauksessa, johon käytettiin LabVIEW-ohjelmalla toteutettua PID-säädintä. Säädintä testattiin nopeiden liikkeiden ohjauksessa ja käytetyt säätömuuttujien arvot määritettiin kokeellisesti. Myös aktuaattorin liikkeen hystereesi mitattiin ja aktuaattorin ajamiseen käytetty virran ohjausyksikkö dokumentoitiin.

TULOKSET: Aktuaattorin nopea liike sekä hystereesi mitattiin. Aktuaattorin liikettä ohjattiin takaisinkytkennän ja PID-säätimen avulla, mutta hyvin nopeissa liikkeissä säätimen puutteet tulivat esiin. Mittauksissa ilmeni myös ongelmia materiaalin mikrorakenteen stabiiliudessa aktuaattorikäytössä. Ideoita ja ehdotuksia esitettiin niin tulevista mittauksista kuin säätimen jatkokehityksestäkin.

JOHTOPÄÄTÖKSET: Huolimatta hystereesin ja nopeiden liikkeiden säädölle asettamista vaatimuksista aktuaattorin nopean liikkeen ohjaus PID-säätimellä onnistui hyvin tai tyydyttävästi. Adaptiivisen säätimen optimointi ja käyttäminen säädössä ratkaisisi useat mittauksissa ilmenneet ongelmat. Tämän lisäksi tarkan säädön toteuttaminen edellyttää muistimateriaalin toistettavaa toimintaa aktuaattoriajossa. Toistettavuuden oletetaan olevan kytköksissä materiaalin mikrorakenteen stabiilisuuteen.

Avainsanat: magneettinen muistimateriaali, PID, säädin, takaisinkytkentä, säätö, aktuaattori

Preface

The work resulting to this thesis was conducted at AdaptaMat Ltd with funding of TEKES. I would like to thank my instructor Juhani Tellinen for introducing me to the world of MSM actuators and for his advice. My grateful thanks also go to Ladislav Straka and Aleksei Sozinov for helpful discussions and guidance in material science. In addition I wish to thank Pekka Mäkelä, Joonas Drebs and Kari Ullakko at AdaptaMat Ltd. I have learned a lot during this project, which means learning about control engineering and material science, but also about perseverance and problem-solving. Furthermore, I would like to acknowledge my supervisor Professor Mervi Paulasto-Kröckel and Markus Turunen from the Laboratory of Electronics Production Technology.

Finally, I give thanks to my friends and family, who all have supported me during my studies, especially my two beloved sisters. However, my greatest thanks go to my fiancé, Akseli, whose love, support and smile have helped me to go this far and always cheer me up.

Helsinki, 24th September 2009

Heini Heikkilä

Contents

List of symbols and abbreviations

a	crystallographic axis
b	crystallographic axis
B	magnetic flux density
c	crystallographic axis
C	transfer function of a controller
D	transfer function of the system to be controlled
e	error between system output and set point
$f(h)$	magnetic driving force
H	magnetic field strength
H_S	saturation magnetic field strength
K_d	derivative control parameter, derivative gain
K_i	integral control parameter, integral gain
K_p	proportional control parameter, proportional gain
K_u	constant of uniaxial magnetic anisotropy
l	length of a MSM sample
l_0	initial length of a MSM sample
M	magnetization
T_C	Curie temperature
T_D	derivative time
T_I	integral time
T_M	martensitic transformation temperature
u	output signal of a PID controller
y	output signal of the system to be controlled
y_{SP}	set point of the control system
χ_m	magnetic susceptibility
σ_{ext}	external compressive stress
σ_{mag}	magnetic stress
$\sigma_{mag,max}$	maximum magnetic stress
σ_{tw}	twinning stress

ε	experimental strain
ε_0	lattice distortion
ε_{max}	maximum strain
μ_0	permeability of vacuum
5M or 10M	five-layered modulated approximately tetragonal martensite
7M or 14M	seven-layered modulated approximately orthorhombic martensite
A/D	analog-to-digital
D/A	digital-to-analog
FPGA	field programmable gate array
EDM	electrical discharge machining
MSM	magnetic shape memory
Ni-Mn-Ga	nickel-manganese-gallium
PID	proportional-integral-derivative
SMA	shape memory alloy
VHDL	VHSIC hardware description language
VHSIC	very-high-speed integrated circuit
vi	virtual instrument

1 Introduction

Magnetic shape memory (MSM) materials have gained attention due to the large shape changes that they can produce in moderate magnetic field (usually < 500 kA / m). Since the discovery of the MSM effect in Ni_2MnGa by Ullakko et al. (1996) this new class of materials has been the target of intensive research. Typically, MSM materials are single-crystalline metal alloys, which convert magnetic energy to mechanical energy. After straining in magnetic field the MSM element can be returned to its initial shape with a mechanical spring or by turning the direction of the magnetic field by 90°.

The particularity of Ni-Mn-Ga compared to other magnetic shape memory alloys is that in this material it is possible to combine large shape changes at a rather high frequency at ambient temperature in moderate magnetic field. Large strains of MSM alloys combined with fast displacements at hundreds of Hertz could be exploited in rapid magnetic actuators and valves. On the other hand, the range of applications is mainly restricted by the martensitic transformation temperature, above which the microstructure required for the MSM effect no longer occurs. Therefore, currently the main focus of the crystal growth development is the elevation of the transformation temperature as well as the reproducibility of material production.

All the Ni-Mn-Ga MSM material and the actuator used in this work were produced at AdaptaMat Ltd. The aim of this work was to document the measurement setup, measure the displacement of a MSM actuator and demonstrate the feedback control of the displacement. Feedback control is used in the control of magnetic valves in order to compensate for the non-linearity and hysteresis typical of magnetic phenomena. In Chapter 2 the theory of the MSM effect and feedback control are introduced. Chapter 3 deals with the measurement system including the actuator, the current module and the realization of the controller. The measurements and results are reported and discussed in chapters 4 and 5, respectively.

MSM materials are closely related to shape memory alloys (SMA), which undergo shape changes up to several percent during heating and cooling. Shape memory alloys also

remember their initial shape. However, the shape changes induced by thermal processes are several orders of magnitude slower than magnetic-field induced shape changes in MSM alloys. Hence, the use of magnetic field and MSM alloys enables fast actuation in applications. The dimensions of a sample can be changed with an external magnetic field also by magnetostriction of ferromagnetic materials. However, generally the strains are one to two orders of magnitude smaller than in the MSM effect (Enkovaara et al. 2004). The piezoelectric materials show strains of order 0.1 % and the magnetostrictive materials can produce strains up to 0.2 %, whereas the reversible strain of the Ni-Mn-Ga MSM alloys in actuator is about 3.5%. Although both types of materials show strains in magnetic field, the phenomena of magnetostriction and magnetic shape memory substantially differ from each other. In MSM the strain is tied to the crystallography through twin boundary motion, whereas in magnetostriction straining occurs only due to the change in magnetization direction (Schwartz (ed.) 2004, p. 936, 949).

2 Theoretical background

Shape memory alloys (SMA) are defined by the property to undergo martensitic phase transformation during cooling, which induces changes in the dimensions of the sample. Additionally, during reverse transformation to the parent phase the sample reverts back to its initial shape and so remembers its shape. Magnetic shape memory alloys are a particular sub-group of shape memory alloys. They exhibit the conventional shape memory effect during heating and cooling, but apart from that single-crystalline magnetic shape memory alloys can produce large shape changes in magnetic field. Magnetic field is used to manipulate the microstructure in the martensite state. Accordingly, in magnetic shape memory effect no crystallographic phase transformations take place as in the conventional shape memory effect. Instead, the MSM phenomenon involves interaction of the microstructure and magnetic domain structure of the sample. More precisely, the actuation in magnetic field is based on the motion of twin boundaries, which causes rearrangement of crystallographic regions in the material (Likhachev et al. 2000).

The first subchapter (2.1) elucidates the martensitic transformation and twinning microstructure of a Ni-Mn-Ga MSM alloy. This is followed by the presentation of the essential magnetic and mechanical properties of the alloy in chapters 2.2 and 2.3 respectively. Chapter 2.4 deals with the reversibility and requirements of the MSM effect.

2.1 Martensitic transformation and twinning in Ni-Mn-Ga

The martensitic transformation is required in order to produce the proper microstructure for the MSM alloy. During slow cooling from 1000 K ordering of Ni-Mn-Ga alloy occurs. At Curie temperature T_C (~100 C°) the magnetic character of the alloy alters form paramagnetic to ferromagnetic. When the material is further cooled a structural phase transformation is observed. It is a lattice transformation from a higher symmetry structure, austenite, to a structure of lower symmetry, martensite (Enkovaara et al. 2004). The

martensitic transformation temperature T_M can vary a lot for different alloys and it is strongly composition dependent (Lanska et al. 2004). The transformation involves shearing deformation and results from the shift of several atoms as a unit rather than individual atoms (Funakubo et al. 1986). The three axes of a rectangular crystal lattice are denoted by *a*, *b* and *c*. In Ni-Mn-Ga the crystal lattice structure is cubic in austenite state, but in martensite state it can be tetragonal, approximately tetragonal or approximately orthorhombic as shown in Figure 1. The non-cubic lattice is an important property in order to obtain large magnetic-field-induced strains.

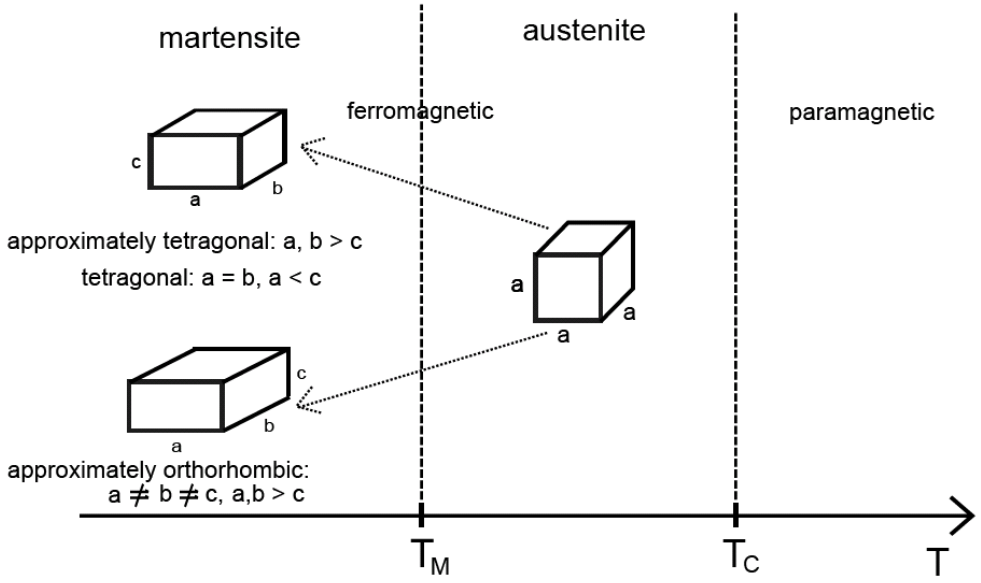

Figure 1 The lattice structures of the austenite and martensite states in a Ni-Mn-Ga MSM alloy. The martensitic transformation temperature is marked by T_M and Curie temperature by T_C.

The formation of martensite lattice structure is diffusionless, thermoelastic and accompanied by shape changes to which the material can accommodate in different ways, for instance by generation of a twinning microstructure. Another possibility for strain adaptation is the formation of slip microstructure involving dislocations. However, the slip microstructure is not usable for the magnetic shape memory effect, whereas the twinned microstructure is crucial for a functional MSM alloy (Funakubo 1986). The twinning microstructure develops in the martensitic phase in order to minimize the interfacial elastic energy over the whole sample (O'Handley 2000, p. 259). Nevertheless, the twinning process does not change the crystal structure of the martensite. As depicted in Figure 2, usually two twin variants with different crystallographic orientations (1 and 2) appear and their regions alternate in the material. The crystallographic lattices of the two twin variants are symmetrically related in terms of a mirror plane or a rotation axis (Otsuka, K. (ed.) 1998, p. 18). The boundaries between different twin regions are even visible by eye on a clear surface of a sample.

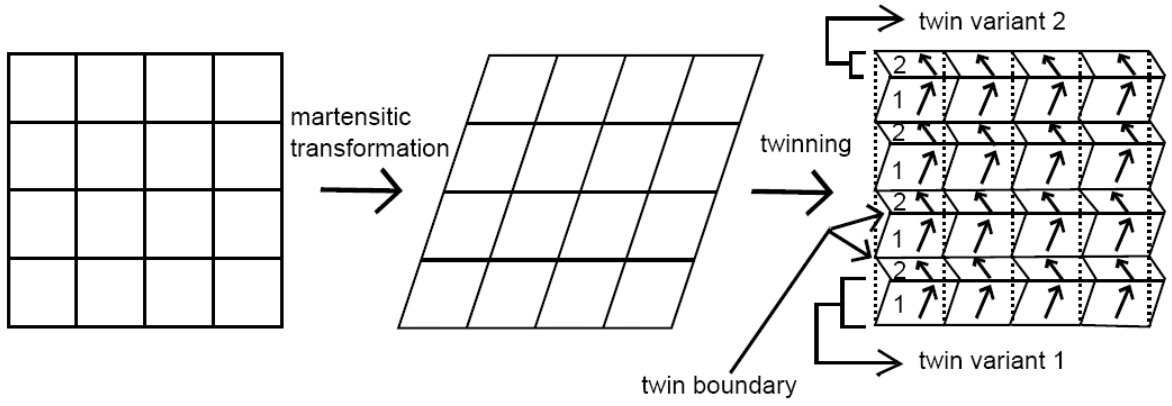

Figure 2 The lattice deformation due to martensitic transformation and subsequent self-accommodation of deformation shear by twinning. In the twinning part of the figure there are twice as many layers of lattices as in the other parts in order to depict the stacking of the structure. The arrows are parallel to the direction of the short axis *c* of the tetragonal lattice.

The different twin variants can have magnetic domains of different orientations. In order to simultaneously minimize the elastic and magnetic interaction energies the martensitic twin orientation domains and the magnetic domains evolve specific patterns (Jin 2009). The magnetic shape memory effect involves growth of the favorably oriented magnetic domains inside a specific twin variant as well as growth of this particular twin variant at the expense of the other variants.

The Ni-Mn-Ga used in this work has approximately tetragonal lattice in the martensite state with lattice parameters a = 0.596 nm, b = 0.594 and c = 0.560 nm and the transformation temperature T_M = 45 C°. For this martensite structure $c < a$, and the maximum theoretical strain is approximately 6 %. This tetragonal lattice structure (referred to as 10M and 5 M in the literature) has only three possible twin variants instead of the six variants of the orthorhombic structure (referred to as 14M and 7M in the literature) (Enkovaara et al. 2004). The 10M designates a specific lattice modulation in the material. In the 10M alloy it is possible to combine large magnetic anisotropy and small twinning stress, which are favorable properties for the MSM effect (Sozinov et al. 2002; Straka 2007, p. 28). In addition, the simple variant structure is a benefit in terms of its controllability. From now on the term Ni-Mn-Ga alloy in this thesis refers to the 10M- structured alloy used also in the measurements reported in chapter 4.

After martensitic transformation Ni-Mn-Ga alloy usually has a multi-variant structure. By applying stress (1-4 MPa) or a magnetic field (~ 500 kA / m) during the transformation the generation of single variant samples can be facilitated. As a result, the variant that appears is the one with the short axis of the crystal lattice along with the strain or the magnetic field (Straka 2007, p. 20-22). The martensitic transformation can be observed by calorimetry as the released or absorbed energy or alternatively by measuring the changes in magnetic susceptibility (Suorsa 2005, p. 22).

2.2 Magnetic properties

The magnetic properties together with the proper crystal structure and microstructure of an MSM alloy enable the magnetic-field induced straining. The magnetization *M* of a material is defined as

$$M = \chi_m H \quad (1)$$

where χ_m is the magnetic susceptibility and *H* the magnetic field strength. The austenite to martensite transformation in Ni-Mn-Ga can be observed as a significant increase in magnetic anisotropy of the material (Suorsa 2005, p.22). The magnetic flux density ***B***, in turn, is related to *M* and *H* as follows

$$B = \mu_0(H + M) \quad (2)$$

where μ_0 is the permeability of the vacuum (4π x 10^{-7} henry / m). Thus, ***B*** is the magnetic flux density that comprises both the external field as well as the field resulting from the magnetization of the material (O'Handley, 2000). The MSM effect involves interaction of the twin domains and the magnetic domains in the alloy. In this respect, the property that lies behind the large strains obtainable in magnetic field is the magneto-crystalline anisotropy of a twinned MSM alloy. (Likhachev, 2000)

A material is magnetically anisotropic, if its magnetization depends on the direction, in which the field is applied to the material. There are several different material properties that can cause magnetic anisotropy, but here we focus on the anisotropy caused by the crystal structure. The physical origin of magneto-crystalline anisotropy derives from the preference

for certain orientations of molecular orbitals or bonding electron charge distributions. As a consequence of magnetic anisotropy single crystal Ni-Mn-Ga in martensite state has an easy and a hard axis of magnetization. This means that the saturation field strength in the easy direction is smaller than in the hard direction (O'Handley 2000, ch 6; Straka et al. 2002). In the material used in this work the easy axis of magnetization is along with the short crystallographic axis *c* and the hard axis along with the axis *a* or *b*. The schematic magnetization curves as a function of the applied field are shown in Figure 3.

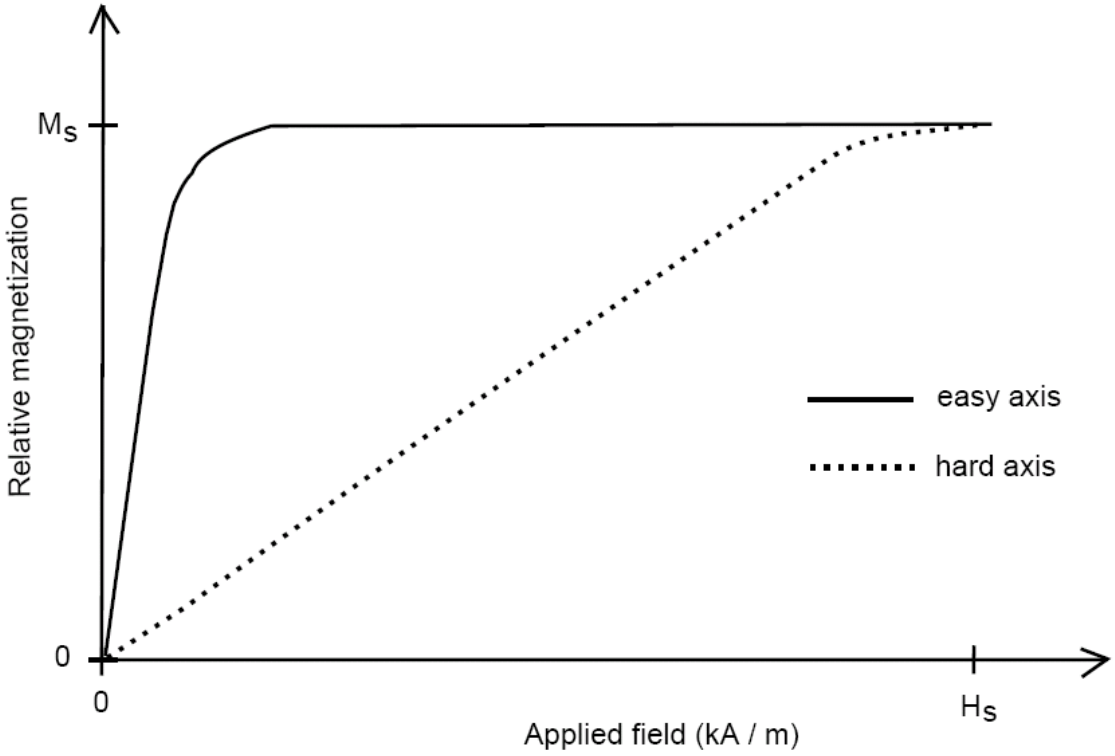

Figure 3 Schematic illustration of typical Ni-Mn-Ga alloy magnetization curves with field direction along with the easy and hard axis of magnetization. The saturation magnetization and magnetic field strength are marked by M_S and H_S (~ 500 kA/m), respectively. Modified after (Suorsa 2005, p. 17).

The area between the magnetization curves in different crystallographic directions represents the magnetic anisotropy energy density (O'Handley 2000, ch. 6). In a single-variant sample the magnetization process caused by a magnetic field along with the easy or hard axis is different. Applying a field transverse to the easy direction results in rotation of the magnetization vector, but when the field is parallel to the easy direction magnetization is caused by the magnetic domain wall motion (O'Handley 1998; O'Handley 2000, p.313).

2.3 Mechanical properties

The experimental strain ε of the Ni-Mn-Ga alloy used in this work was typically 3 %. It is defined as

$$\varepsilon = \frac{(l - l_0)}{l_0} \tag{3}$$

where l_0 is the initial length of the MSM element and l is the length after deformation (Straka et al. 2003). The strain depends not only on the sample length, but also on twinning stress, which is discussed more closely in the following chapter (2.3.1). The crystallographic limit for the theoretical maximum strain is expressed as

$$\varepsilon_{max} = \frac{a}{c} - 1 \tag{4}$$

It is set by the difference between the lengths of the crystal lattice parameters *a* and *c*.

2.3.1 Twinning stress

The blocking forces for twin boundary motion due to material properties are referred to as the twinning stress σ_{tw}. A schematic figure of the stress-strain relationship and one way to determine the twinning stress of the material are shown in Figure 4.

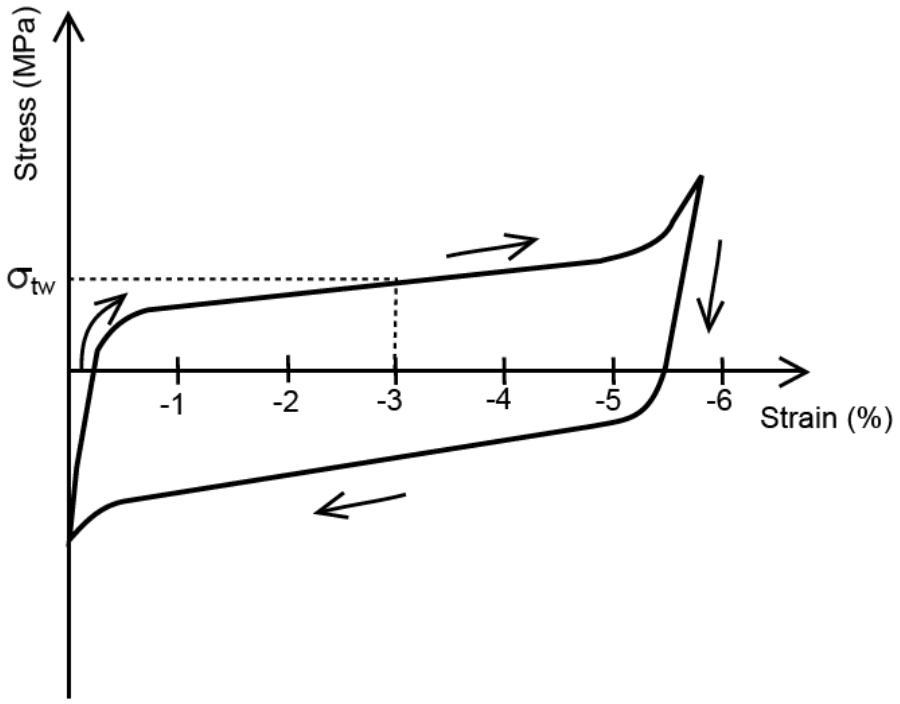

Figure 4 Schematic stress-strain curve of a MSM alloy and the determination of twinning stress as the stress value at 3 % strain of a centered curve.

For a material with a nearly flat plateau of the twinning stress curve the twinning stress value can be approximated to be constant during deformation except for the extremes of the curve. Twinning stress causes hysteresis in the straining behavior and reduces the

magnetic-field-induced stress in the material. In actuator use this implies less force output and efficiency as well as challenging controllability due to hysteresis. Therefore low twinning stress is an important property of a good MSM alloy. However, simultaneously the twinning stress helps the material to keep its shape and thus increases stability in positioning actuator applications (Aaltio 2006). Twinning stress is also strongly dependent on crystal structure and temperature (Sozinov et al. 2003; Lanska et al. 2004). Additionally, twinning stress depends on the purity of the material, crystal quality as well as the thermal, mechanical and magnetic history of the alloy. For example, impurities and defects in the crystal structure tend to increase the twinning stress of the material (Straka 2007, p. 27). Usual twinning stress values for Ni-Mn-Ga MSM alloys vary between 0.2 and 0.7 MPa.

2.4 Magnetic shape memory effect

The magnetic shape memory effect is associated with twin boundary motion between regions that differ in easy magnetization direction (O'Handley 2000, p.259). The important material parameters in order to obtain the MSM effect in an alloy are large magnetic anisotropy, small lattice distortion and small twinning stress (Straka 2007, p.27). All these parameters depend on the crystal structure and temperature, (Sozinov et al. 2002; Sozinov et al. 2003; Heczko et al. 2003). The lattice distortion is defined as

$$\varepsilon_0 = 1 - \frac{c}{a} \tag{5}$$

where *c* is the length of the short and *a* is the length of the long crystallographic axis. Small lattice distortion means smaller maximum strain, but on the other hand big lattice distortion reduces the magnetic stress σ_{mag}, which is needed for the MSM effect. In addition, the magnetic anisotropy that influences the MSM effect depends on the lattice distortion.

2.4.1 Twin boundary motion

Rearrangement of twin variants can be induced by stress or magnetic field. The twin boundary motion caused by mechanical stress brings about large plastic-like deformations by growing the amount of one variant at the expense of another. As a result, the proportion of the variant with the shortest crystallographic axis *c* in the direction of the applied compressive stress grows. Respectively, the twin boundary motion can be initiated by magnetic field, if the martensitic phase has sufficiently strong magneto-crystalline anisotropy. In that case, when the magnetic field is applied the unfavorably oriented twin variants cannot rotate to the direction of the field. Due to the magnetic anisotropy the energy equilibrium is more easily attained by twin boundary motion, that is by growth of the variant with the easy axis of magnetization along with the field (O'Handley 2000, p.265). Figure 5 shows a usual two-twin-variant structure in a MSM alloy in a small magnetic field below the saturation field strength of the easy axis of magnetization (Figure 3). The easy axis of magnetization of the variants is parallel to the dim arrows, which denote the direction of magnetization of each magnetic domain inside the variants.

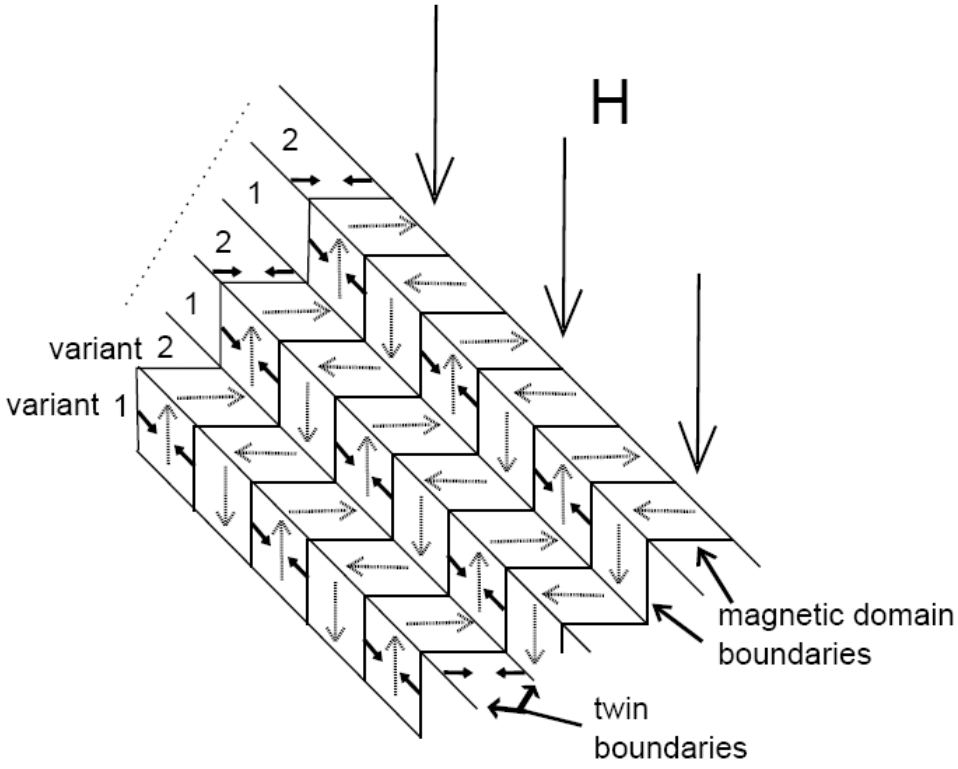

Figure 5 Typical two-twin-variant and magnetic domain microstructure in a Ni-Mn-Ga MSM alloy in a field *H* below the saturation field strength of the easy axis of magnetization. The dim arrows show the direction of magnetization of the magnetic domains. The small dark arrows depict the movement of magnetic domains and twin boundaries in an applied field *H*.

The applied magnetic field in Figure 5 is parallel to the direction of the easy axis of the variant 1. Hence, the MSM effect proceeds by the growth of the magnetic domains of this variant, which are oriented in the direction of the field. This is shown by the solid arrows perpendicular to the magnetic domain boundaries. In addition, the proportion of the favorably oriented crystallographic variant 1 grows at the expense of variant 2 by twin boundary motion. The solid arrows show the direction of the magnetic domain wall and

twin boundary movement. The proportion of the variant 1 is growing along with growing field strength and correspondingly in a bigger fraction of the sample the short axis *c* orientates along with the field and the long axis *a* perpendicular to it. As a result, the sample contracts in its dimension parallel to the field and straining is obtained in a dimension perpendicular to the field.

According to a model created by Likhachev *et al.* (2000) the magnetic driving force *f(h)* applied to twin boundaries equals the difference in the magnetization free energies between the twin variants. The direction of the force is along the normal of the twin boundary. The equivalent magnetic stress σ_{mag} is proportional to the driving force and can be expressed as

$$\sigma_{mag} = \frac{f(h)}{\varepsilon_0} \tag{6}$$

Thus, σ_{mag} is also dependent on the lattice parameters through lattice distortion ε_0. Along with growing magnetic field strength the magnetic driving force approaches its saturation value, which is equal to K_u, the constant of uniaxial magnetic anisotropy. Finally, the maximum equivalent magnetic stress can be written as

$$\sigma_{mag,max} = \frac{K_u}{\varepsilon_0} \tag{7}$$

(Likhachev 2000; Likhachev et al. 2006).

2.4.1 MSM effect in actuator

The MSM effect is usually exploited in actuator applications. MSM alloys can be used in different types of actuator configurations depending on the application. Yet mostly the movement generated by the actuators is cyclic. For example, magnetic field is used to elongate the MSM element and when the field is switched off the mechanical force of a load and a spring is used to return the element to its initial length. Alternatively, a combination of the mechanical force and a force generated by a transverse magnetic field can be used to restore the MSM element.

In a MSM actuator with a spring as the only restoring element the magnetic field pulse is only used to elongate the sample. The spring is compressed during elongation and in order to fully compress the sample it has to apply a stress σ_{ext} greater than the twinning stress σ_{tw} of the material. When the sample is fully compressed a magnetic field pulse is given again to elongate the sample. Thus, the limiting case for reversible MSM behavior is

$$\sigma_{ext} = \sigma_{tw} \tag{8}$$

On the other hand, in order to elongate the sample and to fully reorient its twin structure the magnetic stress generated by the field has to exceed the twinning stress and the external stress of the spring. Consequently, from equation 7 it follows

$$\frac{K_u}{\varepsilon_0} > \sigma_{tw} + \sigma_{ext} \tag{9}$$

Thereby, for fully reversible MSM behavior in actuator the equations 8 and 9 give

$$\frac{K_u}{\varepsilon_0} > 2\sigma_{tw} \quad (10)$$

Equation 9 shows that having MSM material with low twinning stress is a requirement for applications, because low twinning stress decreases the magnetic stress and respectively the magnetic field strength required for strain response (Likhachev 2000; Likhachev et al. 2006).

2.5 Control theory

Feedback loop control and proportional-integral-derivative (PID) controllers are widely used in industrial control applications. The yet simple, but powerful idea of feedback can make a system to follow commands and reduce the effect of disturbances as the real output of the system is continuously compared to its desired value. The first PID controllers date back to the control of steam engines and windmills and their development has proceeded through many shifts in technology. The PID controller still offers a good solution to many practical control problems in small as well as large distributed systems. Mainly PID or PI controllers are used for instance in motor, process and motion control in the industry (Åström 2006).

2.5.1 Feedback loop control

In feedback control the controller is error driven. It receives continuously in its input a measurement of the error *e* between the desired behavior and the actual behavior of the system. The output of the controller is a function of this error. Practically, the controller is

taking corrective action until the error is reduced to zero (Leigh 2004, ch. 3). The principle of feedback control is illustrated in Figure 6, where the required response or set point is marked by y_{SP}, the output of the system to be controlled by y and the error between these two by e.

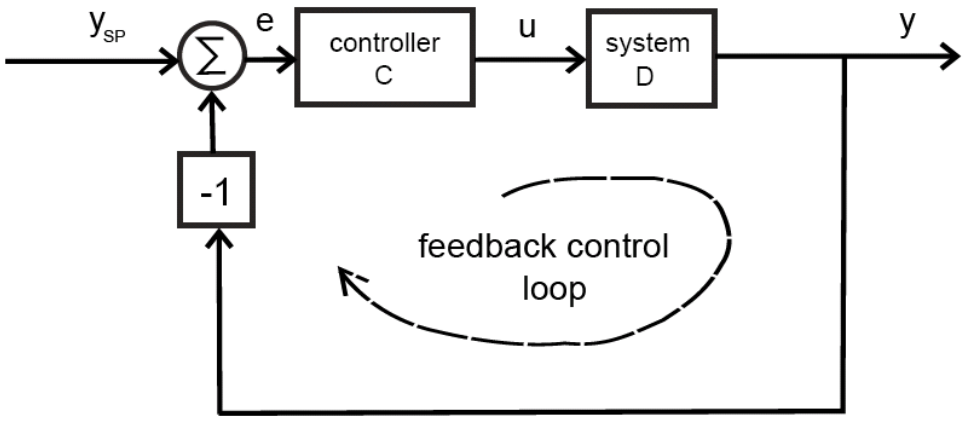

Figure 6 Basic principle of feedback loop control.

The transfer functions of the controller (C) and the system to be controlled (D) represent the relation between their inputs and outputs, respectively. From the flow chart in Figure 6 the following can be obtained

$$y = CDe \tag{11}$$

$$y = CD(y_{SP} - y)$$

$$y = \frac{CDy_{SP}}{(1 + CD)}$$

Finally, the transfer function of the feedback control system can be written as

$$\frac{y}{y_{SP}} = \frac{CD}{(1 + CD)} \tag{12}$$

2.5.2 PID controller

The Proportional-Integrative-Derivative (PID) controller has, as its name indicates, three modes of control. The general mathematical representation of the PID controller is

$$u(t) = K_p e(t) + K_i \int_0^t e(\tau)d\tau + K_d \frac{de(t)}{dt} \tag{13}$$

where K_p is the proportional control parameter or proportional gain, K_i is the integral gain and K_d is the derivative gain. The three terms of the equation 13 correspond to the proportional, integrative and derivative modes of control respectively. The integral gain and derivative gain may be also expressed as

$$K_i = \frac{K_p}{T_i} \tag{14}$$

and

$$K_d = K_p T_d \tag{15}$$

where T_i and T_d are integral time and derivative time in seconds, respectively. From equations 13-15 it is clear that the proportional control parameter K_p is a factor in each term of the PID controller equation. A block diagram representation of the PID controller is illustrated in Figure 7. This diagram corresponds to the controller block in Figure 6.

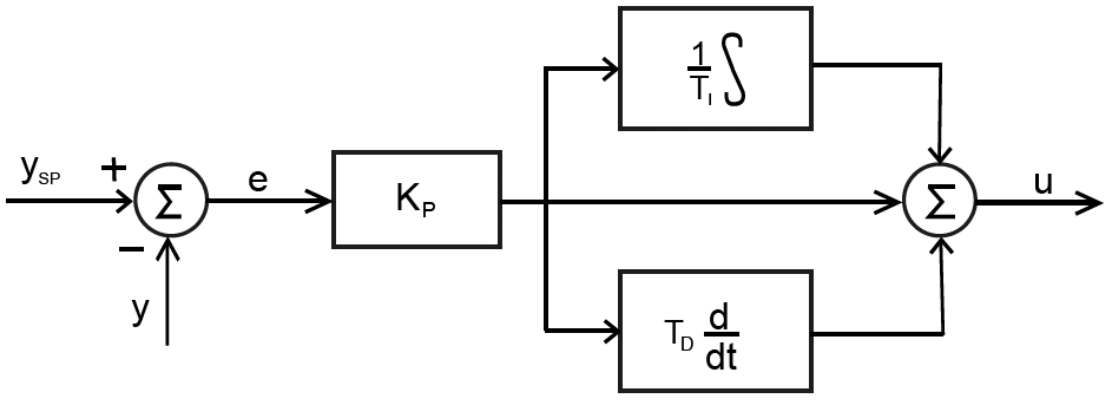

Figure 7 Block diagram of the PID controller. The proportional control parameter K_P is also a factor in the integral and derivative terms.

With only the proportional mode in use the controller output is proportional to the value of the error at its input. Thus, it doesn't make use of any history of its input value or consider the rate of change of this value. The most usual problem of a proportional controller is steady-state offset between the set point and the system output *y*.

The integral control mode shifts the controller output upward, if the control loop error is positive and downward in case the error is negative. The integrator output stays stationary, only if the error is zero. In this way the integral action eliminates the steady-state offset. The effect of the integral mode can be tuned by adjusting the value of the parameter T_i and K_p. The derivative action is based upon the product of K_d and the rate change of the error. T_D is the tuning parameter and the derivative mode is generally used only in combination with P and I modes. It may improve controller's performance by anticipating the effect of load changes and it is often utilized in loops with low noise level and fairly slow response. (Wade 2004)

3 Materials and methods

Two different setups were used in the measurements of this work: one for measuring the displacement of the actuator and another for the feedback control of the displacement. Both setups are presented in this chapter (3.1 and 3.4) as well as the operation of the actuator (3.2). When the actuator is driven a current module is used to generate the current pulses that are fed to the actuator. The current module is described in chapter 3.3, and finally the chapter 3.5 deals with the implementation of the controller used in feedback measurements.

3.1 Setup for measuring actuator's displacement

The MSM elements produce motion and force in magnetic field. The coils of an actuator are used to generate the field and a current control module is needed to drive the actuator. In a basic experiment the current control module produces current pulses that induce a momentary magnetic field in the actuator. Consequently, the MSM elements that are in their compressed state elongate in the field and move the rod of the actuator. In order to measure the movement of the MSM elements a laser sensor is placed above the rod. The measurement setup is depicted in Figure 8. A voltage signal from the function generator is fed into the current module. Generally, a positive rectangular wave signal with an amplitude of 3 V is used. The response of the current module is a nearly rectangular current pulse of current, which induces the magnetic field in the coils of the actuator. The peak value of the current pulse is 3 A.

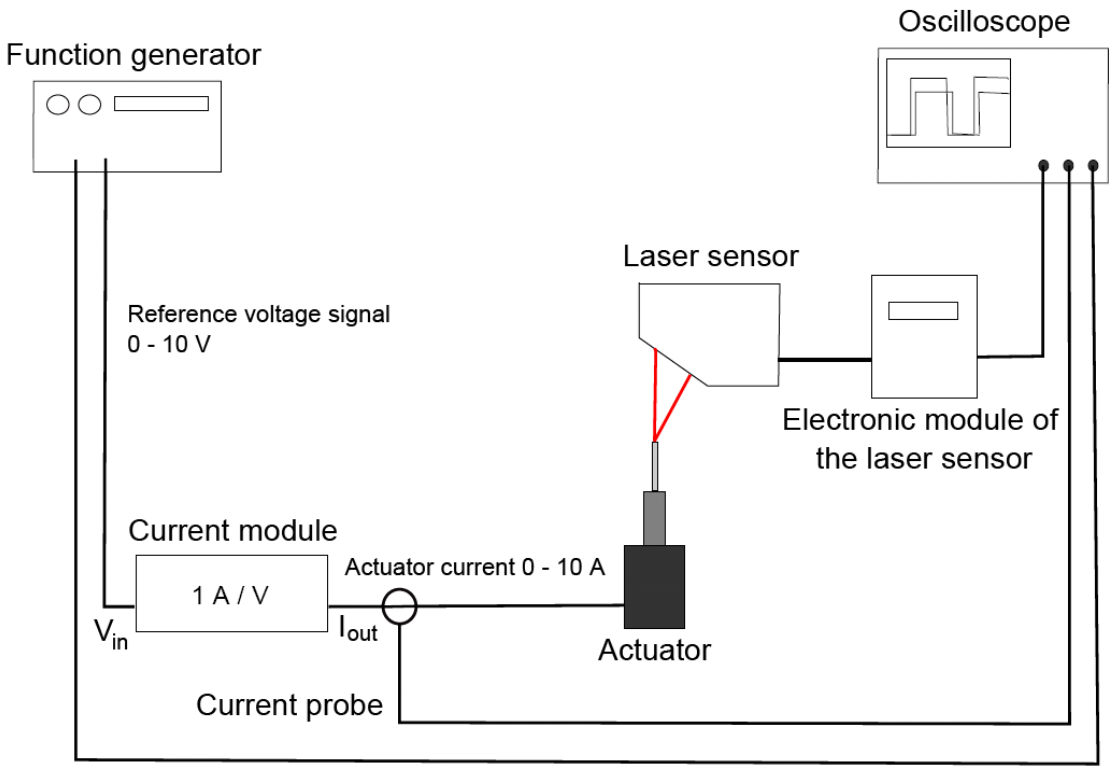

Figure 8 A Setup for measuring actuator's displacement in a pulsating magnetic field with a laser sensor. The actuator current, laser sensor output and reference voltage from the function generator are monitored with an oscilloscope.

The laser detects the displacement of the actuator rod as the MSM elements elongate in magnetic field. The output voltage of the laser sensor is proportional to the displacement of the actuator rod. The input voltage and output current of the current module as well as the laser output voltage are monitored on an oscilloscope.

The laser sensor that was used in the measurements is a triangulation sensor, which incorporates a semiconductor laser and the detection optics. The measurement principle of triangulation is based on the alteration of the angle of reflection from the actuator rod when

the distance of the rod from the laser changes. The Ni-Mn-Ga MSM elements had been cut by electrical discharge machining (EDM), grinded and polished electrolytically. The dimensions of the elements were 1.0 x 2.5 x 20.0 mm and their twinning stress varied between 0.15 and 0.40 MPa. In the actuator 18 mm of the longest dimension of the elements is between the coils in the magnetic field and the elongation is obtained in this dimension.

3.2 MSM Actuator

An actuator retaining two MSM elements was used for the measurements described in this work. The actuator and the elements are shown in Figure 9. The main parts of the actuator include a bottom plate, frame, coils and deck with a pipe and a moving rod. The frame part lies on the bottom plate and is made of 0.2 mm thick iron plates that are adhered together. This structure reduces eddy currents as well as the consequent heating of the material and is commonly used in transformer core construction. Apart from the frame, other parts of the actuator are made of non-magnetic materials. The bottom plate and the deck are aluminum and the moving rod is made of titanium. The temperature inside the actuator can be monitored with a thermocouple during measurements.

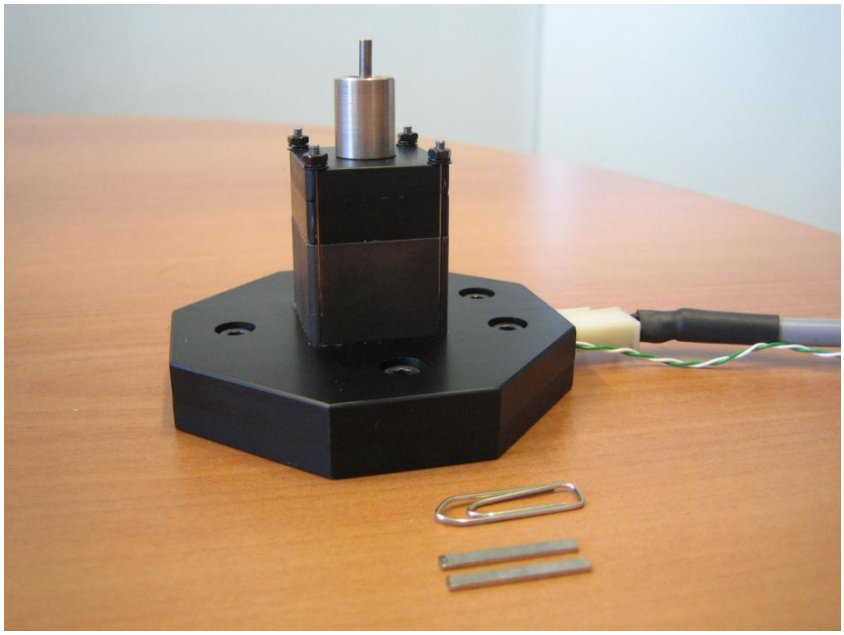

Figure 9 The MSM actuator and two MSM elements in the front. The coils are inside the frame part and the pipe part houses the restoring spring.

Two coils are placed inside the frame part and there is a groove between them for the elements. The operation of the actuator is depicted in Figure 10. When a magnetic field is applied the elements elongate in the groove pushing the rod upwards. The inner surfaces of the groove are teflonized in order to decrease friction of the movement. The pipe part houses a spring, which acts as a restoring force. When the MSM element elongates the spring is compressed, subsequently recovering and enforcing the element to shrink when the magnetic field is removed.

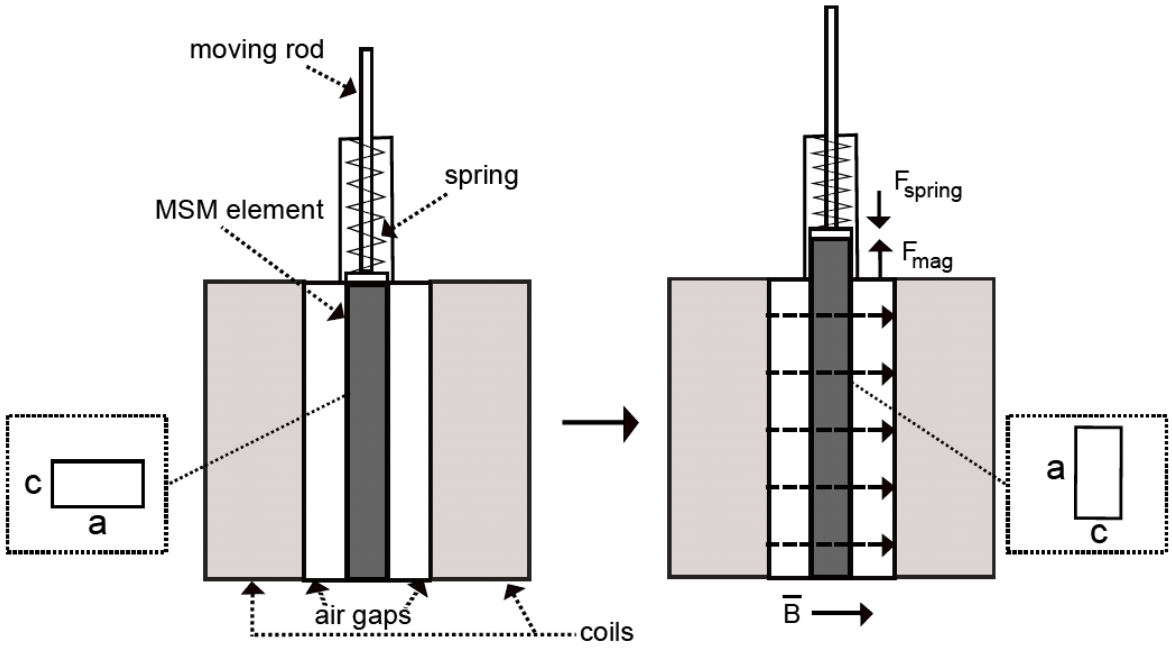

Figure 10 Operation of the MSM element in an actuator. The insets indicate the orientation of the most prevalent twin variant in each situation. The sizes of the air gaps and elements are exaggerated.

A spring with a spring constant of 0.5 N / mm was used. The space for the spring can be shortened and the spring pre-stressed by adjusting a screw in the pipe part. The coils are wired in parallel.

3.3 Current module

In order to drive the actuator the current control module is used to generate current pulses according to the reference signal of the function generator. For instance, when quadratic

voltage pulses are used as a reference signal the current control module outputs nearly quadratic current pulses to the coils of the actuator. The current control module comprises a DC brush servo amplifier circuit, which is modified to give a current of 1 A per 1 V of reference voltage. The circuit diagram of the current module is shown in appendix I.

First the reference voltage from the function generator is sensed by a differential amplifier with a gain G_1 = 1 and then preamplified by G_2 = - 0.3. At the output of the voltage follower the voltage becomes the demanding signal which controls the pulse width modulation (PWM) stage. The design of the circuit determines that the demand signal produces 20 A in the output of the PWM for 6 V in the output of the voltage follower. Thus, the demand ratio is 20 A / 6 V = 3.3 A/V and it is the same for the output current sense. The gain G_2 of the preamplifier multiplied with the demand ratio give the final ratio of 1 A output current for 1 V reference voltage. The current error amplifier compares the current reference with the output current monitor and adjusts the output voltage according to the current demanded. The PWM stage acts then as a current source and converts the current demand into a current in the actuator.

In order to reduce the current ripple at the switching frequency of the PWM stage (f = 25 kHz) a LC filter was introduced in the output of the amplifier circuit. The ripple creates excess eddy currents in the actuator, thus heating it and elevating the ambient temperature of the elements. As the MSM effect is temperature-dependent (Heczko 2003; Straka et al. 2006) all additional heating should be avoided. Because currents up to 4 A are regularly used to drive the actuator, inductors with adequate current rating had to be chosen for the filter. On the other hand, the higher the inductances, the more they degrade the transient response of the current module output. A LC filter circuit with L_S = 100 mH and C_S = 1μF was used and is shown in appendix I.

3.4 Feedback control setup

In feedback control measurements a PID controller was used to regulate the reference voltage of the current module. The control system is shown in Figure 11. The set point signal y_{sp} represents the position to which the actuator rod is wanted to move. The controller input signal is the error e between the set point signal y_{sp} of the function generator and the laser signal y. Both of them are voltage signals and the aim is to control the displacement of the actuator so that it follows the set point. The controller regulates its output voltage in order to keep the error e as small as possible. The output voltage of the controller is fed into the reference input of the current module, which generates the corresponding current. This way the current fed to the actuator is adjusted according to the set point and the previous measurement of the actuator's position.

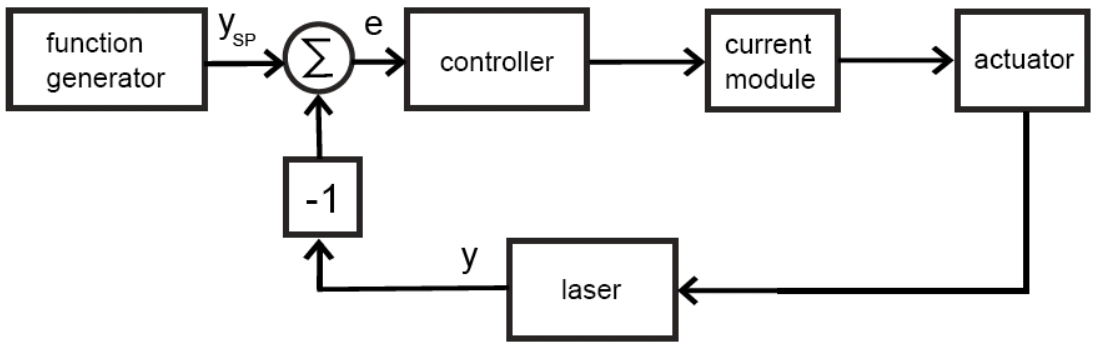

Figure 11 Block diagram of the feedback control setup.

The P, I and D coefficients of the controller equation were experimentally adjusted for each measurement. Due to the testing character of the work experimental tuning was chosen instead of system modeling or application of specific tuning rules. Finally, the derivative mode was not observed to bring any advantage in the measurements and only the P and I terms of the controller were used (equation 12).

3.5 Implementation of the controller

The controller was realized with LabVIEW program running on National Instruments CompactRIO hardware. This platform was chosen due to the possibility to realize simple PID loops with over 100 kHz loop update rate and due to the later modifiability of the system.

3.5.1 Controller hardware

The cRIO-9074 integrated hardware platform included a 400 MHz real-time processor, a 2M Gate FPGA (Field Programmable Gate Array) and two I/O modules: an analog-to-digital (A/D) voltage input (9215) and a digital-to-analog (D/A) voltage output (9263) module with 16-bit resolution. The device was connected to the host computer via network cable. The FPGA part of the hardware consists of a matrix of reconfigurable gate array logic circuitry. Configuration of the FPGA creates a hardware implementation of the software application by using programmable interconnect switches between the logic gates. The operations on a FPGA are truly parallel, because they are directly implemented on hardware and they don't have to compete for the resources of an operating system (NI Application Note 2006).

The hardware platform containing the FPGA chip was chosen due to the requirement of high closed loop update rate. A high update rate naturally improves the performance of the controller, since it enables the controller to react quickly to abrupt changes in the error.

Because the FPGA chip is directly connected to the inputs and outputs of the hardware platform, the highest loop update rate and fastest execution of the PID algorithm were obtained when the PID controller was realized directly on the FPGA.

3.5.2 Controller software

The program consisted of three parts: the FPGA.vi (virtual instrument), the real-time RT.vi and host.vi. The host.vi is executed on the processor of the host computer, whereas the RT.vi executes on the real-time processor of the cRIO hardware platform. The purpose of the RT.vi was to mediate information between FPGA.vi and host.vi.

In the FPGA.vi input voltage values were read, the output of the PID algorithm was calculated and written to the output of the voltage module. These functions were executed in a loop with loop time of 6 μs. The FPGA.vi was constructed in LabVIEW development system and translated into VHDL (Very-high-speed integrated circuit Hardware Description Language) before the transfer and execution on the cRIO hardware. In order to ensure as fast execution as possible the FPGA.vi program had to be kept simple. The programs of all the three virtual instruments are shown in appendices II-VII.

The host.vi includes the user interface of the program, where the user can change the control parameters, initialize and stop the controller. The program is waiting for front panel activity from the user before it executes further and mediates the specific command to the RT.vi. Then the RT.vi reads the variables that were updated by the host and passes the new PID parameter values or the initialization command to the FPGA.vi.

4 Measurements and results

In the first chapters the measurements of the displacement (4.1) and hysteresis (4.2) of the actuator are presented. These measurements were made in order to document the properties of the actuator. The following chapter (4.3) considers the feedback control measurements. The aim of the control measurements was to test the performance of the basic PID controller in MSM actuator control as well as to demonstrate the feedback control of a MSM actuator's displacement. In this work the term rise time is used for the time that a ramp signal needs to rise from its zero level (OFF) to its final (ON) level. The fall time is defined likewise, but from the maximum (ON) level to the zero (OFF) level. The dead-time, in turn, is determined as the delay time between two signals and duty cycle (in percents) refers to the fraction of the period during which a pulsing signal is on.

4.1 Measuring the displacement of the actuator

The displacement of the actuator was measured with the setup shown in Figure 8. A periodic rectangular wave pulse of 3.0 volts at the frequency of 30.0 Hz and duty cycle of 10 % was fed into the current module. Thus, the pulse with a period of 33.3 ms was on for 3.3 ms and off for 30.0 ms during each cycle. Figure 13 depicts the response of the current module and the displacement of the actuator.

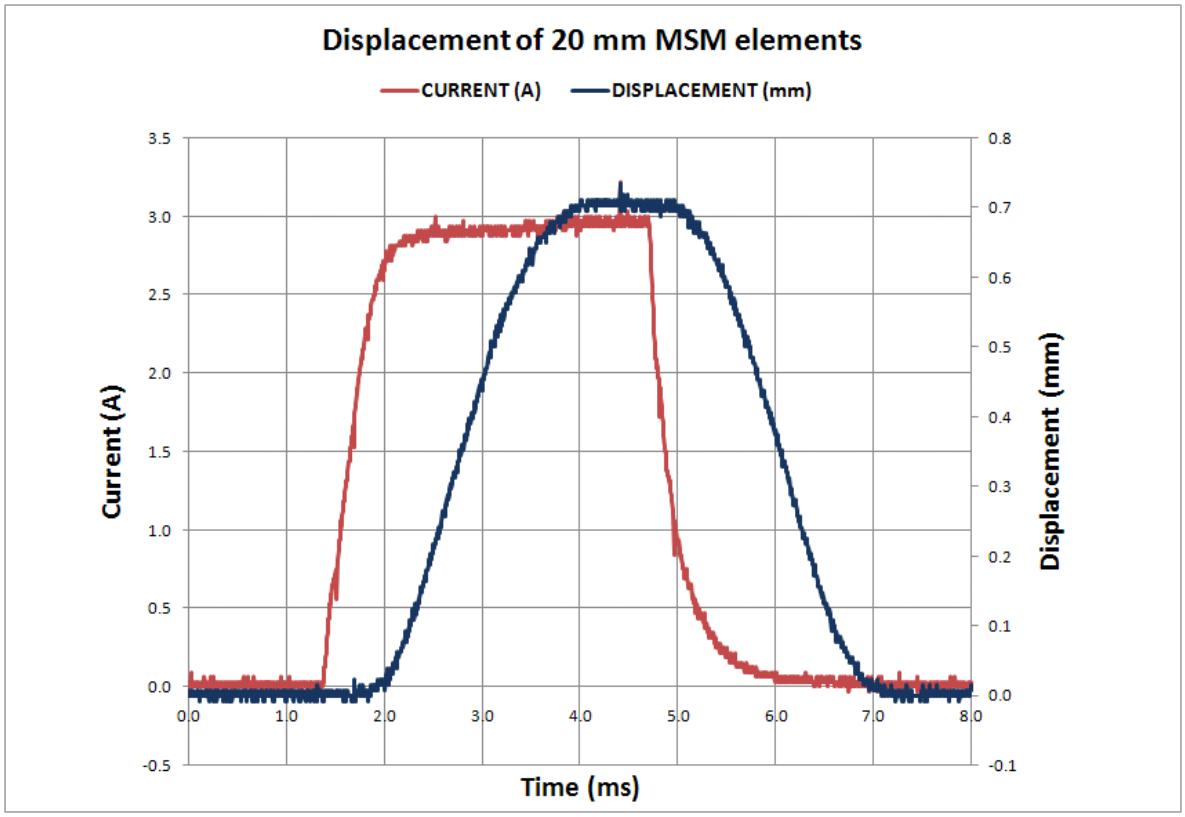

Figure 13 The current pulse and actuator's response during a fast displacement of 0.7 mm in 2.1 ms.

The response of the current module corresponds to the 3.3 ms reference voltage pulse that was used. The pulse is nearly rectangular in shape with a little rounding of two edges. The rise time of the current module is 0.7 ms and the actuator has reached its maximum displacement 2.1 ms later. The falling edge of the current pulse rounds up towards the end and the fall time of the actuator is again 2.1 ms. The dead-time between the current pulse and the displacement signal is 0.5 ms at the rising and 0.3 ms at the falling edge. Even faster displacements, like 0.7 mm in 1 ms, are possible, but then the inertial force often causes a peak of overshoot at the end of the rising displacement. The peak is due to the high

acceleration that the elements and the actuator rod attain, and the rod tends to continue its movement after the MSM elements have stopped straining. The overshoot peak can be diminished by setting the restoring spring tighter, but this also increases the stress that the elements have to overcome before they start straining. In Figure 13 the high spring pre-stress prevents the displacement from overshooting, but on the other hand it increases the current value at which the straining starts (~ 2.7 A). Therefore the spring pre-stress influences also the delay between the displacement and the current.

The rise time of the current module sets the upper limit of usable pulse frequency when driving the actuator. When the frequency is too high the current module isn't able to raise its output fast enough and the current pulses are no longer rectangular in shape. Lowering the duty cycle of the reference voltage signal to 10 % decreases the time that the pulse is on and consequently reduces heating of the actuator due to eddy currents in the frame part and the resistance of the coils. Hence, generally a duty cycle of 10 % was used in all the measurements.

4.2 Hysteresis of the MSM actuator

Hysteresis of strain in pulsing magnetic field is an inherent property of MSM materials due to their twinning stress. A hysteresis curve of current versus displacement of the actuator is shown in Figure 14. The curve was measured with the setup in Figure 8.

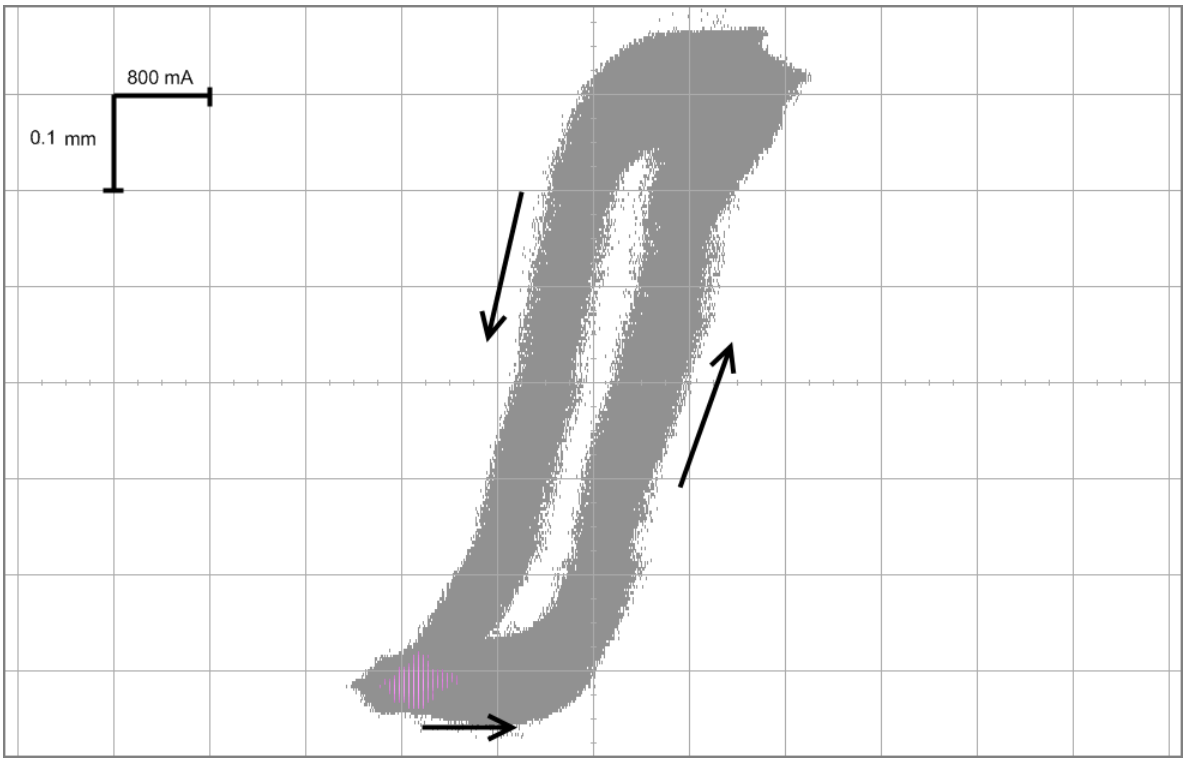

Figure 14 Current-displacement hysteresis curves measured with positive sinusoid signal as the current. The amplitude of the signal was 3.0 A and the frequency 1.0 Hz. One loop corresponds to a period of the sinusoid signal.

The curve was measured using a positive sinusoid signal with 3.0 A amplitude at a frequency of 1.0 Hz. The loop corresponds to one period of the sine signal. The arrows indicate the direction of the hysteresis loop starting from the left-hand lower corner of the curve in Figure 14. As the current starts increasing the displacement first stays at zero, but then increases as well. Similar behavior is observed at the maximum displacement when the current decreases. This results to the different paths of displacement as the current grows and decreases.

4.3 Feedback control of actuator's displacement

The measurement setup and control software presented in chapters 3.4 and 3.5 were used in the feedback control measurements. The measurement reported in chapter 4.1 demonstrated that the MSM elements could respond to a current pulse and strain to their maximum displacement in 2.1 ms. The aim of the feedback control measurements was to test, whether equally fast displacements could be produced and simultaneously controlled. Each control measurement started by tuning of the PID controller parameters. An experimental tuning procedure was chosen due to the demonstrative character of the work. It turned out that the best results were obtained when only the P and I modes were used. The tuning started by increasing the value of the K_p parameter until the system was no longer stable. Then at a stable K_p parameter value the K_i parameter was incrementally increased.

In the measurements the inputs of the controller are the set point signal in volts and the voltage signal of the actuator's displacement from the laser. In most of the figures of this chapter the displacement and the set point are shown in millimeters so that they are easily comparable. The conversion ratio is 2 V / mm. In the measurements without feedback control the function generator signal is directly the reference voltage of the current module and the current is thus practically equal to the function generator signal. On the contrary, in the measurements with feedback control the current is adjusted by the controller in order to minimize the error between the set point and the displacement. The control signal in the figures of this chapter is the controller output signal.

4.3.1 10 ms rise in the set point pulse

A voltage ramp of 1.0 V was used as the set point signal with the feedback control setup and control software described in chapters 3.4 and 3.5 respectively. The rise time of the ramp from 0 to 1.0 V was 10.0 ms. Figure 15 shows the set point signal from the function generator and the displacement of the actuator.

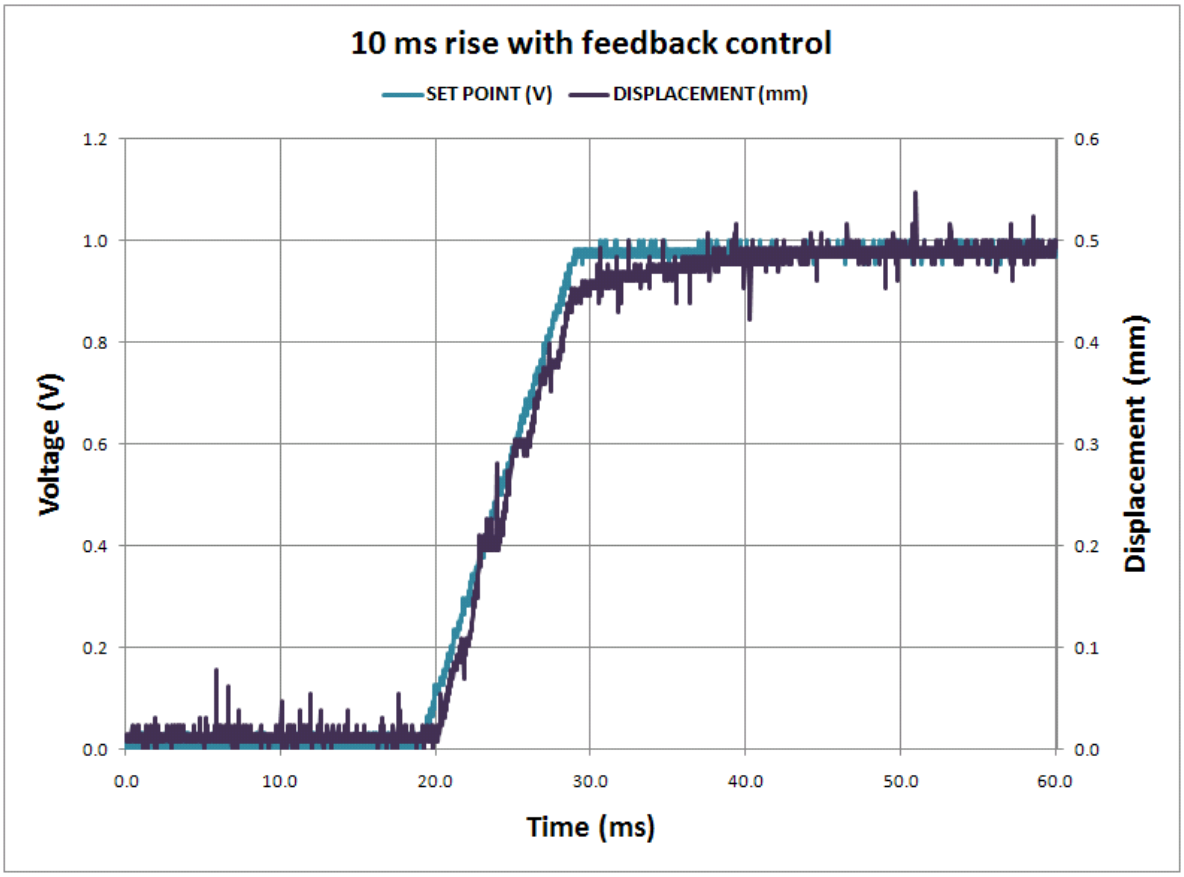

Figure 15 10.0 ms ramp as a set point signal and the displacement of the actuator with feedback control.

The PI controller parameters in the measurement were K_p = 8.0 and K_i = 0.016. With these parameter values the actuator's displacement neatly follows the set point signal. Clearly, the displacement of the actuator has some delay, which is mainly due to the time constant of the actuator. In the displacement signal the edge of the ramp is rounded and the displacement little by little approaches the final value of 0.5 mm. However, there isn't any remarkable steady-state error or overshoot at the edge of the ramp. By careful inspection of

the displacement curve a stepwise growth of the displacement can be observed. This indicates that the MSM elements tend to elongate too fast and override the set point. The control system has to decelerate the growth of the current as it detects that the displacement starts to be close to the set point. Thus, the material should be able to easily follow also steeper set point ramps as also the measurement in chapter 4.1 demonstrates. In order to demonstrate the effect of the feedback control system a similar measurement without feedback control is illustrated in Figure 16. Now a ramp that rises in 10.0 ms to 3.0 V was used as the voltage reference signal.

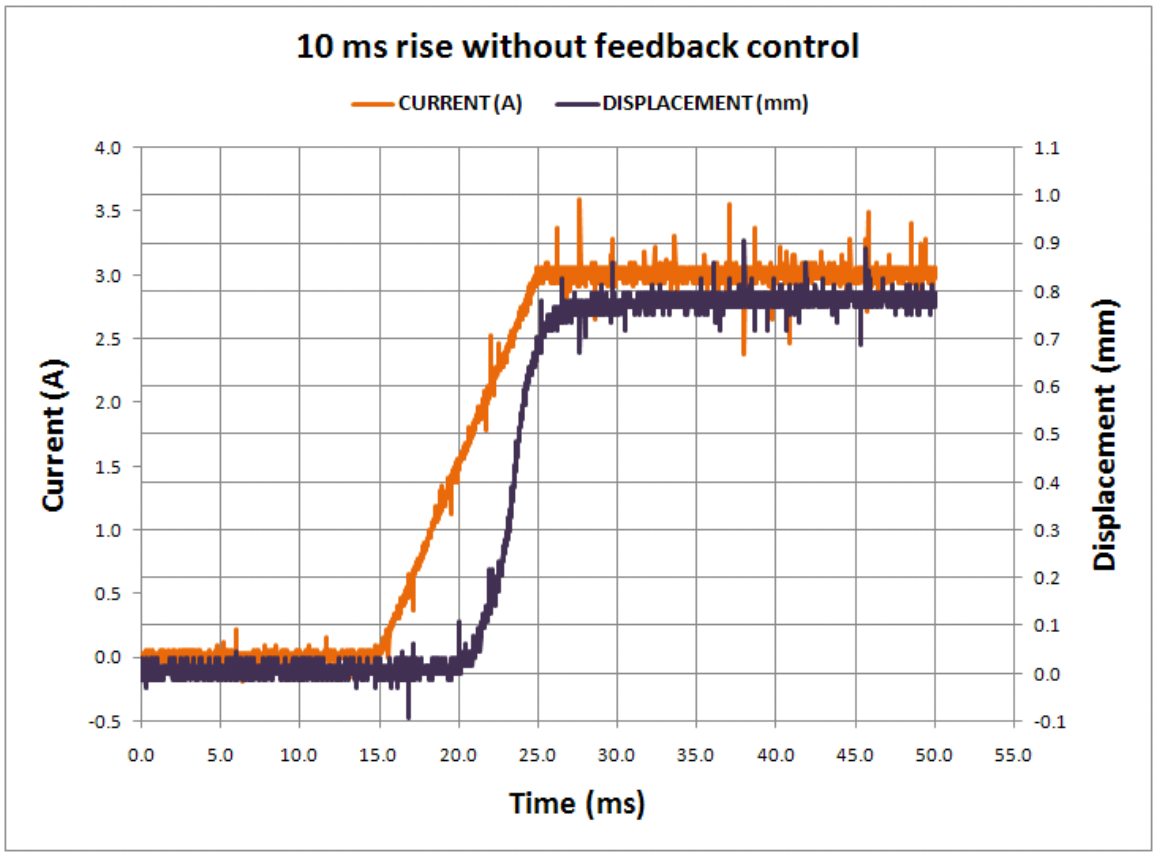

Figure 16 Current and displacement of the actuator with a 10.0 ms rising ramp signal without feedback control. The elements do not start elongating before the current has reached the value of 1.4 A.

The curves in Figure 16 were obtained with the setup for measuring actuator's displacement described in chapter 3.1. The current curve is shown instead of reference voltage (or set point) in order to point out that there is no set point in this system like in the one with feedback control. Instead, Figure 16 shows the true response of the actuator to the current curve rising in 10.0 ms. The delay of the displacement is notably bigger (~5 ms) than in the measurement with feedback control (Figure 15). Straining of the MSM elements is observed first at a current of 1.4 A. Hence, with a current curve of 1.0 A maximum value that the set point curve of Figure 15 would have produced the elements wouldn't strain at all. A bigger current is needed to produce a strong enough magnetic field in order to exceed the twinning stress of the elements and the pre-stress of the spring. Naturally, if the slope of the reference voltage and corresponding current curve would be steeper, the delay of the displacement would also be smaller. Next the performance of the control system was tested with faster rising ramps.

4.3.2 2 ms rise in the set point pulse

A 300 ms lasting set point pulse of 0.35 mm maximum displacement was used as the set point. The rise and fall time between 0.0 mm and maximum displacement is 2.0 ms. The whole pulse with respective control, current and displacement signals is shown in Figure 17. The PI parameters used in the measurement were K_p = 6.0 and K_i = 0.012.

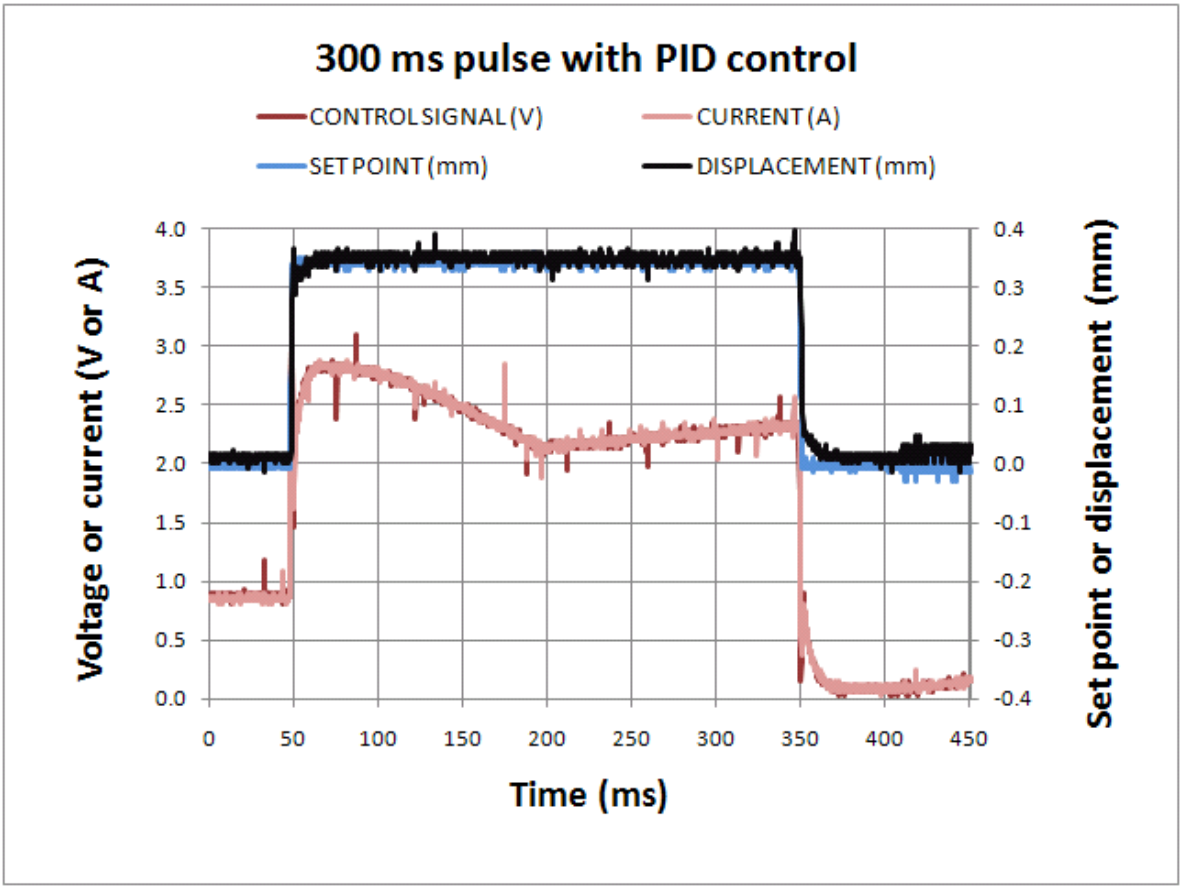

Figure 17 A 300 ms set point pulse with rise and fall time of 2.0 ms. The respective control signal, current and displacement are shown as well.

The current curve is following neatly the control signal and the displacement seems to follow the set point as well. The next figures (18 and 19) elucidate more closely the falling and rising edges of the pulse. In Figure 18 the 30 ms time window of 38 – 68 ms of Figure 17 is depicted.

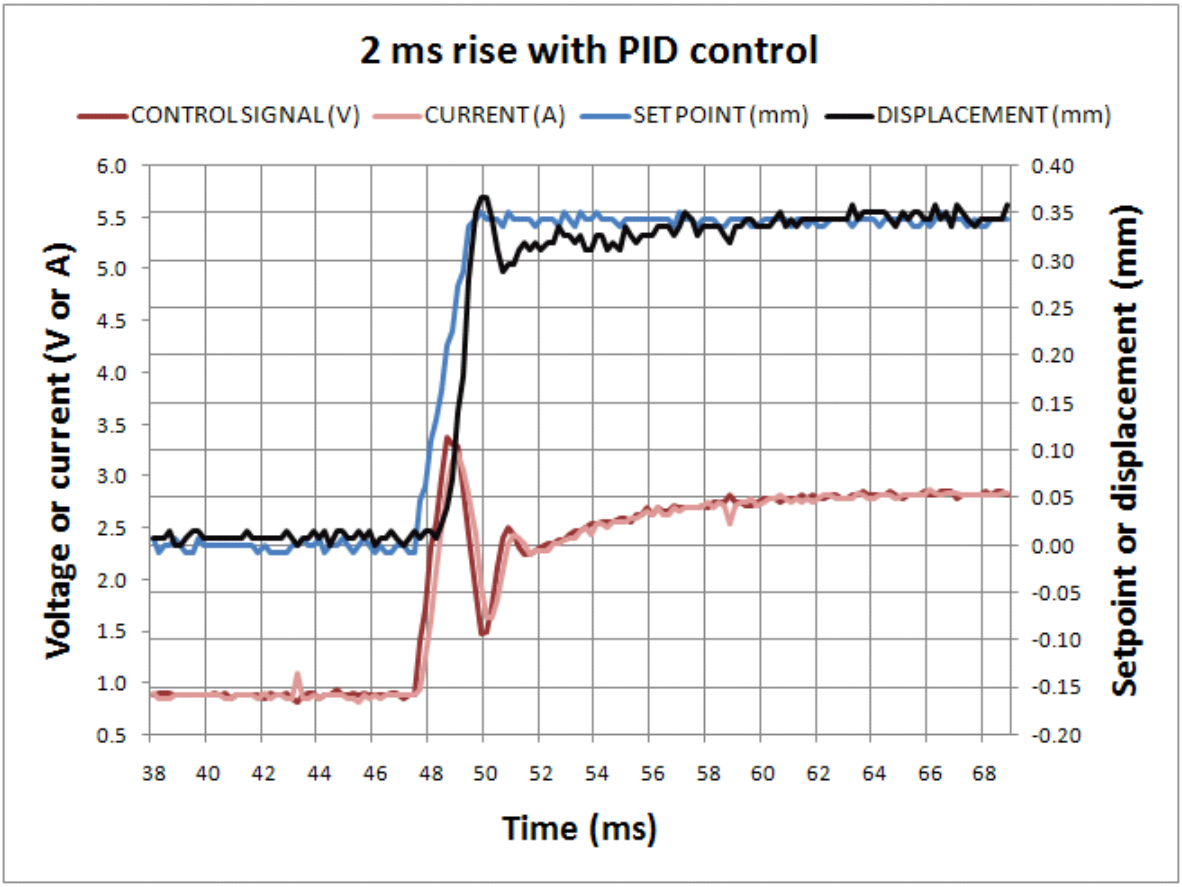

Figure 18 The edge of the set point pulse rising in 2.0 ms and the respective current, control signal and displacement.

The set point signal rises in 2.0 ms and the control signal followed by the current immediately reacts to the growth of the error between set point and displacement. The growth of the error increases both the proportional and the integral terms of the controller output (equation 13). The displacement reacts to the growing current and as soon as the error starts diminishing the output of the controller decreases. However, despite of the controller's reaction overshoot of the displacement occurs at the edge of the ramp before

the displacement starts decreasing. The growth of the error is seen as a new spike in the controller signal at ~51 ms. The controller corrects the current and respectively the displacement starts to grow approaching slowly the constant set point value. With the controller presented in this work it was not feasible to control the 2.0 ms rise without overshoot or alternatively without a delay of several milliseconds in the displacement at the beginning of the ramp. A more detailed discussion of possible further development of the controller is given in chapter 5. Figure 19 zooms in the falling ramp in the time window of 340 to 370 ms of Figure 17.

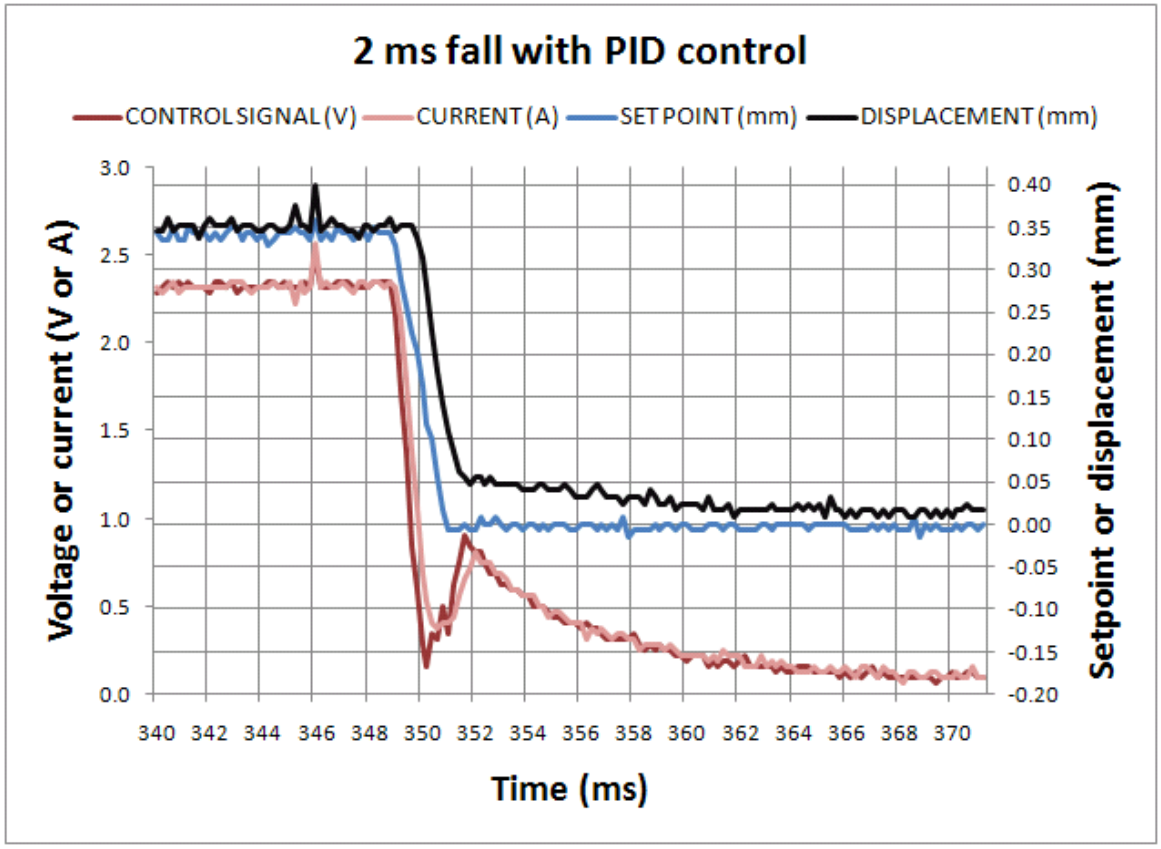

Figure 19 The edge of the set point pulse falling in 2.0 ms and the respective current, control signal and displacement.

As the negative error starts growing the controller signal rapidly decreases, first due to the negative proportional term and then due to the decrease of the integral term. However, just after the time point 350 ms the error starts to diminish as the elements pushed by the spring begin to gain on the set point. The controller responds to the decreasing negative error by increasing its output. Consequently, the spring doesn't fully compress the sample and the displacement curve slowly approximates the set point as the current decreases again. This kind of control behavior rounds up the edge of the falling ramp as can be seen in Figures 17 and 19. Particularly, it may cause problems when the time between pulses is short, in this case less than 20 ms.

Finally, the displacement doesn't reach the set point value, but stays at 0.2 mm. Often this constant error just kept on growing during the measurements and finally the elements showed only a fraction of their initial strain. The incomplete contraction of the sample caused variation in the zero level of the displacement, which is problematic from the control point of view. Reasons and possible solutions to these and other problems that arose during the measurements are discussed in chapter 5.

4.3.3 Two-step rising ramp with feedback control

The control system was finally tested with a more challenging ramp function. As shown in Figure 20 the curve rises to 0.5 mm in two 0.25 mm steps, which last 2.0 ms each. Between the first and the second rising ramp the curve stays at 0.25 mm for 24.0 ms and finally at 0.5 mm for 70.0 ms. Then the set point decreases back to zero in 2.0 ms.

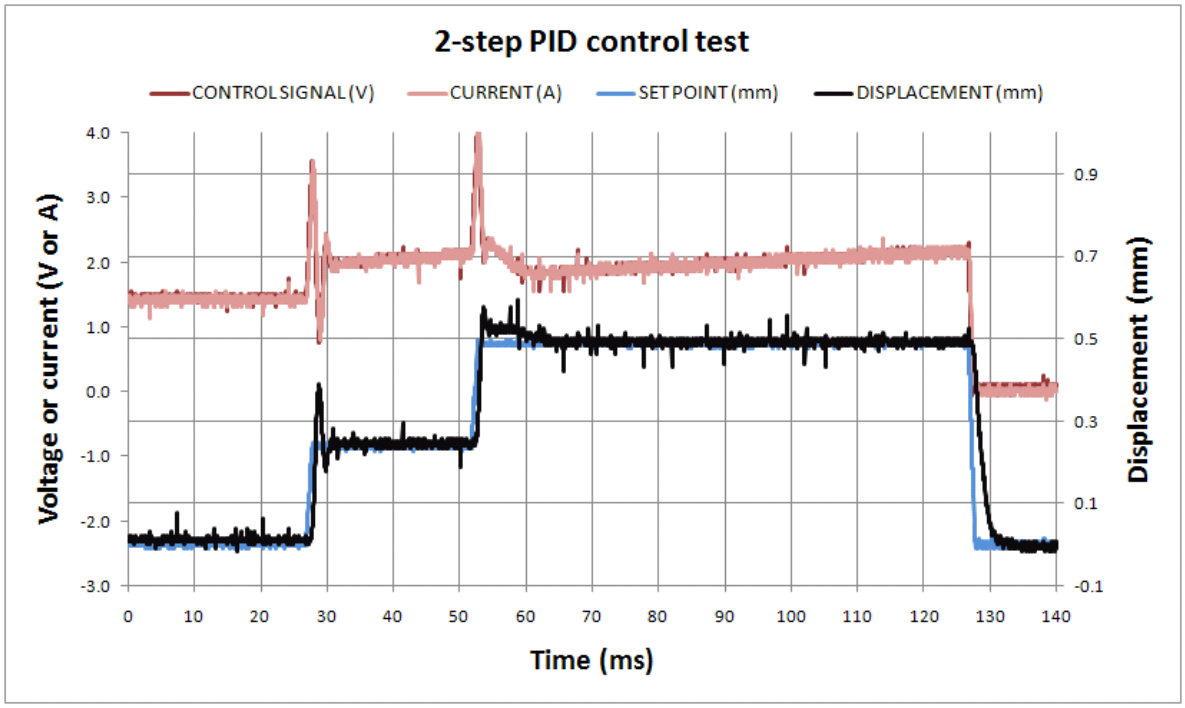

Figure 20 Measurement with the set point curve rising in two steps.

The best results shown in Figure 20 were obtained with PI values K_p = 4.0 and T_i = 0.012. The rounding of the falling edge in the displacement curve is similar to the earlier measurements (Figure 17 and 19). In this respect, the accurate control of the falling ramp with a simple PID controller seems more challenging than the control of the rising ramps. The rising ramps are shown in more detail in Figure 21.

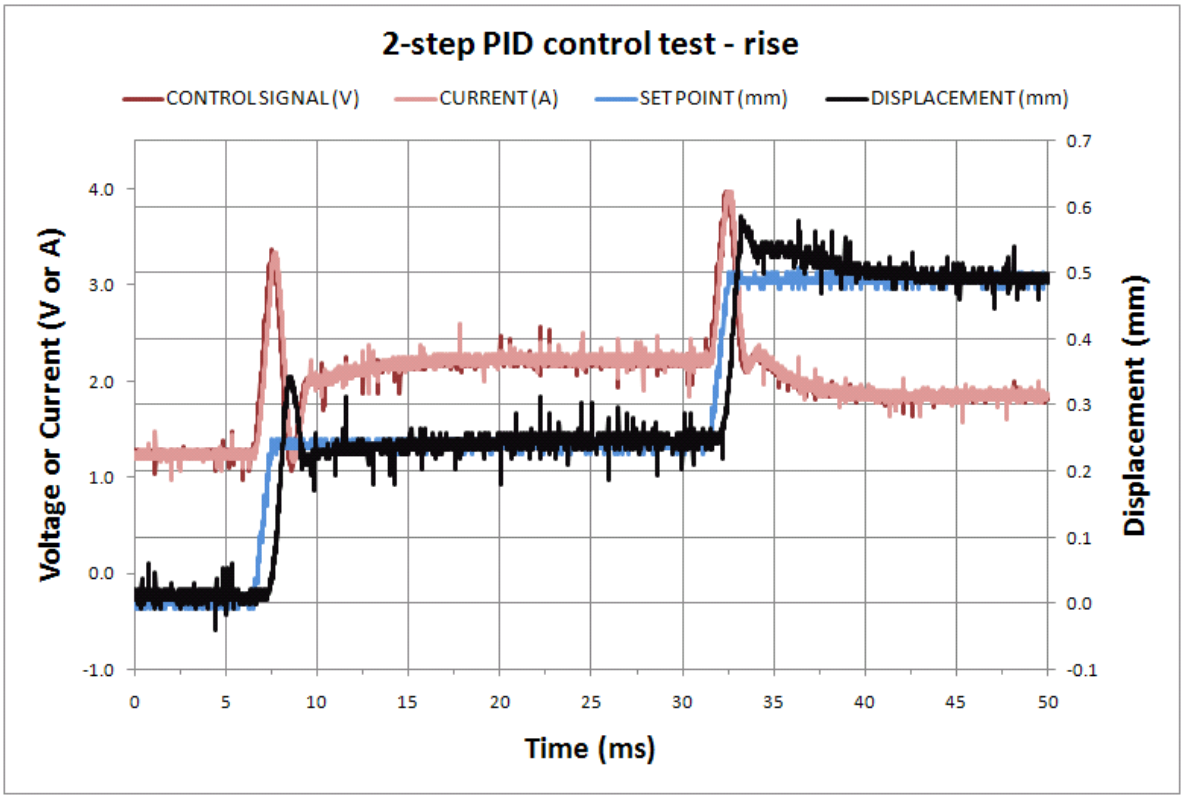

Figure 21 A closer view of the rise in two steps. The displacement overshoots at both steps.

The first rising ramp is harder to manage for the control system and produces a zigzag pattern in the current. Yet the displacement settles quickly compared with the second ramp, where the displacement slowly approaches its final value. Interestingly, the current tended to stay at over 1.0 A even when the set point was 0 mm. This indicates that the element was not fully compressed during previous measurements, because current was needed to keep the element at 0 mm displacement.

5 Discussion

The displacement of a MSM actuator with pulsing movement and the current-displacement hysteresis curve were measured with a laser sensor. A PID controller was successfully used to control the displacement of the actuator with ramp functions rising in 10.0 and 2.0 ms. Problems that arose during the control measurements as well as the stability of the MSM element microstructure are discussed in chapter 5.2. Additionally, ideas for the development of the controller and further measurements are presented.

5.1 Measurement of actuator's displacement and hysteresis

The 20.0 mm MSM elements produced a 0.7 mm (3.5 %) strain in 2.1 ms. This demonstrates the extremely fast nature of the MSM effect. When measuring the actuator's displacement the maximum frequency of the current pulse is restricted by the rise time of the current module. The component values of the current error amplifier affect the rise time as well as the inductive loads of the ripple filter and the actuator. Additionally, rounding of the falling ramp of the current pulse limits the maximum frequency of pulsing. The current has to exceed a certain threshold value before the elements start straining. This is visible in the measurements of chapters 4.1 and 4.2.

Heating of the actuator easily becomes a problem during measurements. As several key parameters in the MSM effect (chapter 2.4) depend on temperature, a constant ambient temperature would be desirable for stable behavior of the MSM elements in actuator. Additionally, if the temperature rises above the martensitic transformation temperature the material loses its MSM properties. The actuator is heated by the eddy currents in the ferromagnetic core and by the dissipated heat due to the straining of the MSM elements. Also the coils produce heat during operation of the actuator. In pulsing mode operation the duty cycle of the pulses can be kept low (~10 %) in order to diminish the heating caused by eddy currents and the coils. Also the ripple filter at the output of the current module reduces

heating by decreasing the ripple current amplitude. In response to heating the triangle and sinusoid signals have more favorable form factors than square wave pulses, but practically the simple on/off movement produced by rectangular wave is the one used in many applications (Unitrode Application Note 1999). The actuator construction can also be further developed in order to increase the dissipation of heat from the core. For instance, the core can be shaped in order to provide a larger surface for heat dissipation or the parts next to the elements in the actuator can be machined from a material with low thermal conductivity. However, using a material with low thermal conductivity next to the elements would also prevent the dissipation of the heat produced by the elements.

The current-displacement hysteresis curve was measured and shown in Figure 14. Due to the twinning stress of the MSM material there is a threshold value of magnetic field strength, which has to be exceeded in order to observe straining of the elements. In other words, the magnetic stress has to overcome the twinning stress and the spring stress before straining starts. In Figure 14 the threshold current value at which this occurs is approximately 1.4 A. Similarly, at maximum current (~3 A) the current can be decreased by a certain amount without any changes in the strain. The twinning stress is again resisting the twin boundary motion and now the contraction of the elements. Hence, the spring is working against the twinning stress and the magnetic stress, which means that the magnetic stress has to diminish sufficiently in order for the elements to start contraction. Therefore, lowering the twinning stress of the material also narrows the hysteresis curve and diminishes the threshold current region. At this point it is also noteworthy that the twinning stress depends on strain and is not constant over the cycle of straining. At higher frequencies the inertial forces of the actuator rod affect the measurement of the displacement, because of the high acceleration of the elements once they start straining in magnetic field. However, the measurement of Figure 14 was done at 1 Hz in order to demonstrate the static properties of the actuator.

The hysteresis also contributes to the damping abilities of the MSM material. In fast movements the inertial force often causes a peak of overshoot in the displacement of the actuator. This is usually followed by vibration of the mechanical system, which generally is problematic in applications. However, the hysteresis of the MSM material dampens the unwanted mechanical vibrations due to the high internal friction of the material. Additionally, the hysteresis reduces the effect of current higher harmonics, which cause heating through eddy currents in the actuator core. Alternatively, the hysteresis may improve the power efficiency of the actuator also in positioning applications, where it might lower the current needed to keep the actuator in a certain position. As a result, in position controlled systems the hysteresis is advantageous in vibration damping in fast displacements, but due to hysteresis the MSM actuator requires a sophisticated controller design for accurate control of fast displacements.

5.2 Feedback control measurements

The 10 ms measurements (Figures 15 and 16) show that despite of the fast nature of the MSM effect, it is also feasible to let the actuator satisfactorily follow a more slowly growing set point signal. However, finally the heating of the actuator causes problems, if too long pulses are used. The effect of the feedback control is demonstrated and it clearly diminishes the delay at the beginning of the displacement by adjustment of the current. Without feedback control a significant delay occurs, because a certain current value has to be exceeded before the MSM elements show straining. At the edge of the ramp the MSM elements manage fairly well the sharp change in the set point signal without overshoot.

During tuning of the controller parameters the system occasionally became unstable, and the controller output as well as the current started oscillating. As a result, the actuator quickly heated up several degrees before the control system was shut down. The heating could be decreased by setting an upper limit to the controller signal (and current), but nevertheless the overheating made the tuning process time-consuming. Additionally, due to

the variation in the properties of the sample material (e.g. twinning stress), the controller parameters had to be retuned for every new pair of elements. This also made repeating of the measurements challenging.

In the measurements with rising ramps in 2.0 ms overshoot occurs with PID controller parameters that let the elements follow reasonably well the set point during the rest of the rise. Due to the hysteresis the current has to be strongly increased in the beginning of the ramp in order to start the straining of the elements. However, after a sluggish start the MSM effect proceeds fast and overshoot often occurs. The overshoot might be avoidable by decreasing the integral parameter K_i, but this would also increase the delay during the rise. In the measurements with the set point rising in two steps the displacement overshoots at both steps. However, during the first step, the requirement to exceed the threshold current before straining makes this step more demanding to control than the second one. As a result, the controller produces a zigzag-like pattern before the displacement settles.

The drawback of the simple PI controller used in the measurements is that the proportional tuning parameter K_p, once set, remains constant for large as well as small errors. By using an adaptive controller the value of K_p could change dynamically depending on the error. This would obviously improve controller performance as the K_p parameter would be increased for small values of the error, as for instance in the beginning of the ramp, enabling the control system to respond faster to them. The lag of the displacement at the beginning of the ramp and possibly also the overshoot would be diminished as the controller output would increase and decrease faster. Now the reaction time of the controller output is limited by the growth and decrement of the integral and proportional terms. Additionally, a model of the hysteresis behavior of the MSM material could be included in the controller algorithm to improve its behavior even further.

At the falling ramp the spring often couldn't totally compress the sample, which created problems during the measurements. Partial compression resulted in the shift of the zero level of the displacement and degraded the performance of the control system. Gradually, the overall strain of the elements also diminished. The reason for decreased ability of the

spring to compress the elements is intricate. There is a peak in the first decreasing controller signal, which causes the current to grow at the end of the ramp. Although the consequent field isn't strong enough to produce any displacement it produces magnetic stress in the elements. This stress is acting against the restoring spring probably by braking its movement. Possibly, also the slope in the set point (and current) curve would decrease the inertial force that normally adds to the restoring force at fast compression. Hence, the conclusion would be that due to the diminished restoring force the compression is incomplete and that with sloping set point ramps the spring force has to be bigger than usual for full sample restoration. This would mean that the maximum reversible strain would be diminished due to the slope, but contradictorily the compression was incomplete even when the displacement in the 2.0 ms measurement was only half (0.35 mm) of the normal maximum displacement of the elements used in the measurements.

On the other hand, the fact that in some identical measurements the compression attained the zero level of displacement during some cycles before incomplete compression occurred indicates that the reason for partial compression would be rather an alteration in the variant microstructure of the elements. The nucleation of new variants might increase the twinning stress and diminish the maximum strain obtained. Interestingly, this kind of behavior was rarely observed when the elements were driven with rectangular pulses without feedback control. It implies that during feedback control the elements would be subject to conditions that would tend to change the microstructure of the material. Further tests should be made using sloping pulses with and without feedback control and with different values of the spring pre-stress combined with inspection of the microstructure. Finally, also the improvements of the controller described in the previous paragraph would probably ease the control of the falling ramp as the fluctuations in the error signal, and thus also in the controller output, would be smaller.

Also the recovery of the elements after diminished strain varied. The strain of some samples could be recovered in actuator by pulsing with 3.0 A rectangular current pulses for 10 minutes. Some samples were fully or partially recovered after training of a few cycles of extension and compression by hand. Even more interestingly, a few samples seemed to

recover just with time when they had not been used. And finally there were also samples that didn't recover at all. Some of those samples had visible cracks or two opposing boundaries, which are known to hinder the MSM effect at least partially. The exact reasons to the different recovery behavior of the samples are unclear and need to be examined further.

6 Conclusions

The displacement of the MSM actuator was measured as well as its hysteresis. The PID controller was successfully applied to the feedback control of the displacement. The control results with pulses rising in 10.0 ms were good and with rises of 2.0 ms satisfactory. The hysteretic current-strain dependency makes the accurate control of fast displacements demanding. Diminished maximum strain and partial compression of the elements caused problems during the control measurements. The reasons and possible solutions to these problems were discussed. Also ideas for future measurements and improvement of the controller were presented.

The problem of actuator overheating during tuning of the controller might be avoided by design and application of a proper tuning procedure based on the controller values that performed well in this work. Also the use of a more sophisticated adaptive controller and elements with reproducible material parameters would ease the tuning. However, the most important step would be to clarify, whether the microstructure of the elements is altered in the actuator and in which conditions this happens. The principle aim in the future is to get control of the microstructure in such a way that the operation of the elements in actuator is stable. Finally, this knowledge can be applied to control measurements.

References

Aaltio, I. & Tellinen, J. 2006, "Deformation Properties of Magnetic Shape Memory Materials used in Actuators", *Proceedings ACTUATOR 2006*10th international conference ACTUATOR 2006, Bremen, Germany 14-16th June.

Åström, Karl J. & Hägglund, Tore 2006, *Advanced PID control*, ISA - Instrumentation, Systems, and Automation Society, NC. ISBN 1-55617-942-1.

Enkovaara, J., Ayuela, A. & *et al*. 2004, "Magnetically driven shape memory alloys", *Materials Science and Engineering A,* vol. 378, no. 1-2, pp. 52-60.

Funakubo, H. (ed.) 1986, *Shape memory alloys*, Gordon and Breach, New York. ISBN 2-88124-136-0.

Heczko, O. & Straka, L. 2003, "Temperature dependence and temperature limits of magnetic shape memory effect", *Journal of Applied Physics,* vol. 94, no. 11, pp. 7139.

Jin, Y.M. 2009, "Domain microstructure evolution in magnetic shape memory alloys: Phase-field model and simulation", *Acta Materialia,* vol. 57, no. 8, pp. 2488-2495.

Lanska, N., Soderberg, O. & *et al*. 2004, "Composition and temperature dependence of the crystal structure of Ni-Mn-Ga alloys", *Journal of Applied Physics,* vol. 95, no. 12, pp. 8074-8078.

Leigh, J.R. 2004, *Control theory,* 2nd ed. edn, Institution of Electrical Engineers, London. ISBN 1-60119-074-3.

Likhachev, A.A., Sozinov, A. & et al. 2006, "Modeling the strain response, magneto-mechanical cycling under the external stress, work output and energy losses in Ni-Mn-Ga", *Mechanics of Materials,* vol. 38, no. 5-6, pp. 551-563.

Likhachev, A.A. & Ullakko, K. 2000, "Magnetic-field-controlled twin boundaries motion and giant magneto-mechanical effects in Ni–Mn–Ga shape memory alloy", *Physics Letters A,* vol. 275, no. 1-2, pp. 142-151.

NI Application Note 2006, *National Instruments, FPGA-based control: Millions of transistors at your command (FAQ)*, National Instruments Corporation.

O'Handley, R.C. 1998, "Model for strain and magnetization in magnetic shape-memory alloys", *Journal of Applied Physics,* vol. 83, no. 6, pp. 3263-3270.

O'Handley, R.C. 2000, *Modern magnetic materials, Principles and applications,* Wiley, New York. ISBN 0-471-15566-7.

Otsuka, K. (ed.) & Wayman, C.M. (ed.) 1998, *Shape memory materials,* Cambridge University Press, Cambridge. ISBN 0-521-44487.

Schwartz, M.M. (ed.) 2004, *Encyclopedia of smart materials,* Knovel, Norwich (NY).

Sozinov, A., Likhachev, A.A. & et al. 2002, "Crystal structures and magnetic anisotropy properties of Ni-Mn-Ga martensitic phases with giant magnetic-field-induced strain", vol. 38, no. 5, pp. 2814-2816.

Sozinov, A., Likhachev, A.A. & et al. 2003, "Effect of crystal structure on magnetic-field-induced strain in Ni-Mn-Ga", *Smart Structures and Materials 2003: Active Materials: Behavior and Mechanics. Proceedings of the SPIE Volume 5053*, ed. Edited by Lagoudas, Dimitris C, , pp. 586.

Straka, L. & Heczko, O. 2003, "Superelastic response of Ni-Mn-Ga martensite in magnetic fields and a simple model", *IEEE Transactions on Magnetics,* vol. 39, no. 5, pp. 3402-3404.

Straka, L., Heczko, O. & et al. 2006, "Temperature dependence of reversible field-induced strain in Ni-Mn-Ga single crystal", *Scripta Materialia,* vol. 54, no. 8, pp. 1497-1500.

Straka, L. 2007, *Magnetic and magneto-mechanical properties of Ni-Mn-Ga magnetic shape memory alloys,* Helsinki University of Technology, Espoo.

Straka, L., Heczko, O. & et al. 2002, "Magnetic Properties of Various Martensitic Phases in Ni-Mn-Ga Alloy", *IEEE Transactions on Magnetics,* vol. 38, no. 5, pp. 2835-2837.

Suorsa, I. 2005, *Performance and Modeling of Magnetic Shape Memory Actuators and Sensors,* Helsinki University of Technology, Espoo.

Ullakko, K., Huang, J.K. & et al. 1996, "Large magnetic-field-induced strains in Ni_2MnGa single crystals", *Applied Physics Letters,* vol. 69, no. 13, pp. 1966-1969.

Unitrode Application Note 1999, *A high precision PWM transconductance amplifier for microstepping using Unitrode's UC3637 (U-112),* Texas Instruments.

Wade, H.L. 2004, *Basic and advanced regulatory controlsystem design and application,* ISA-The Instrumentation, Systems, and Automation Society, Research Triangle Park, NC.

APPENDIX I: Circuit diagram of the current module

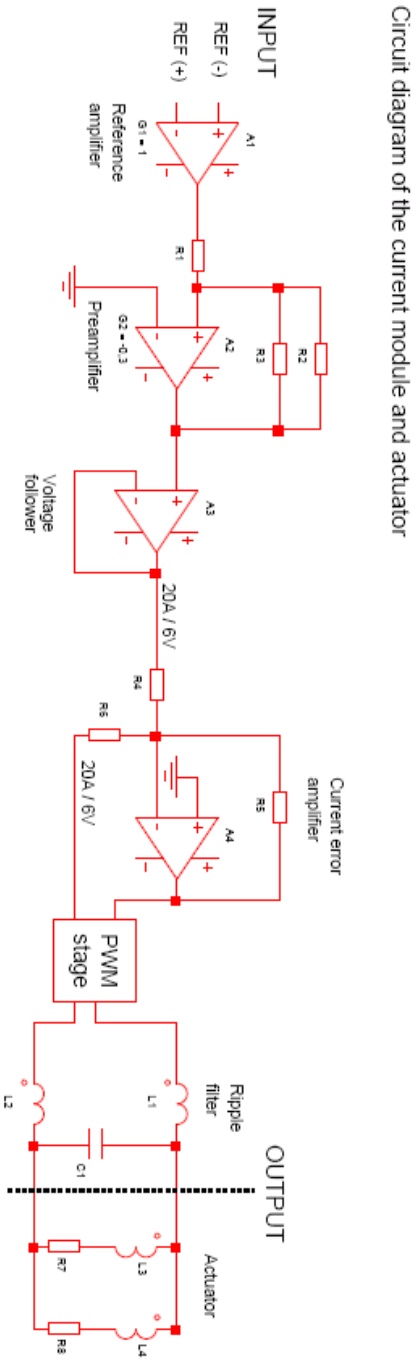

APPENDIX II: FPGA.vi block diagram

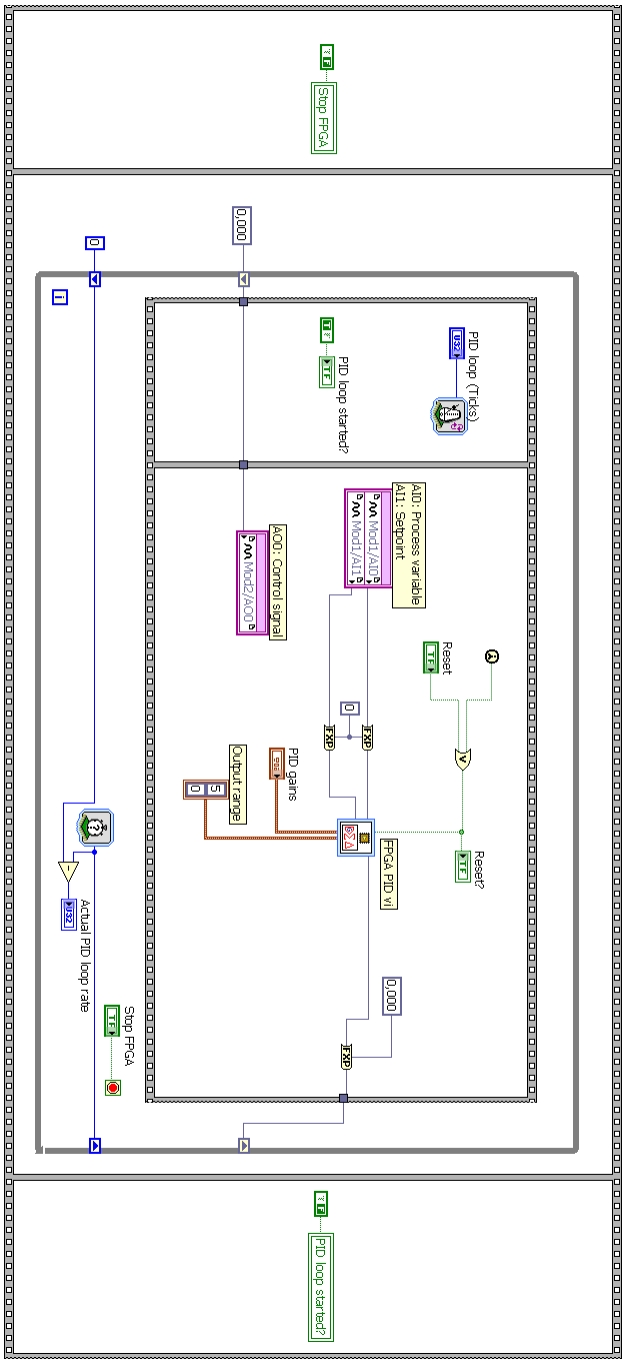

APPENDIX III: RT.vi block diagram, part 1

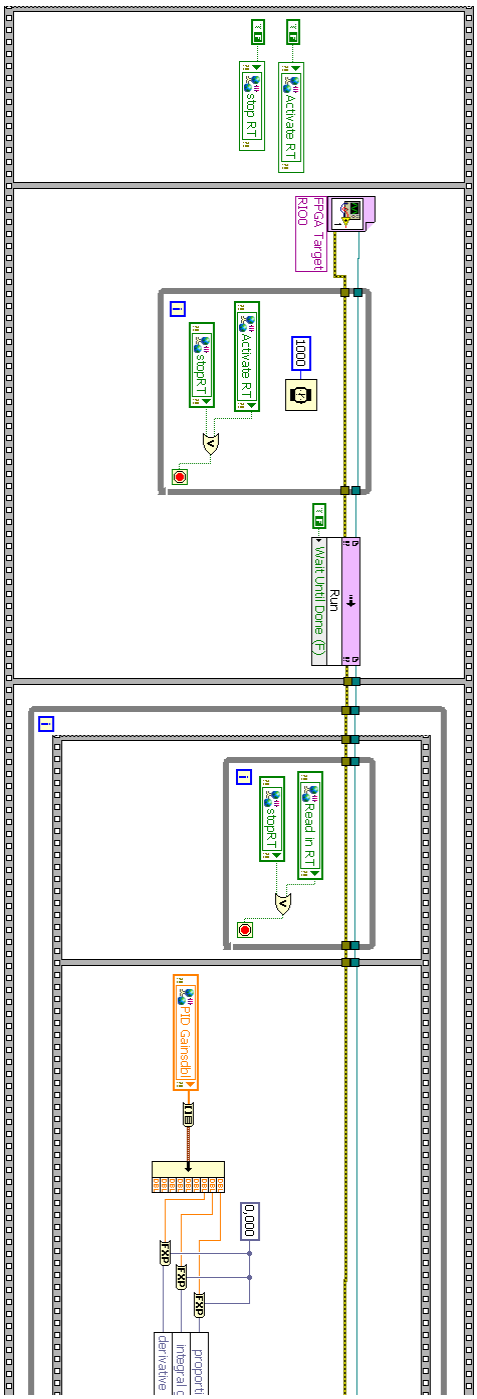

APPENDIX IV: RT.vi block diagram, part 2

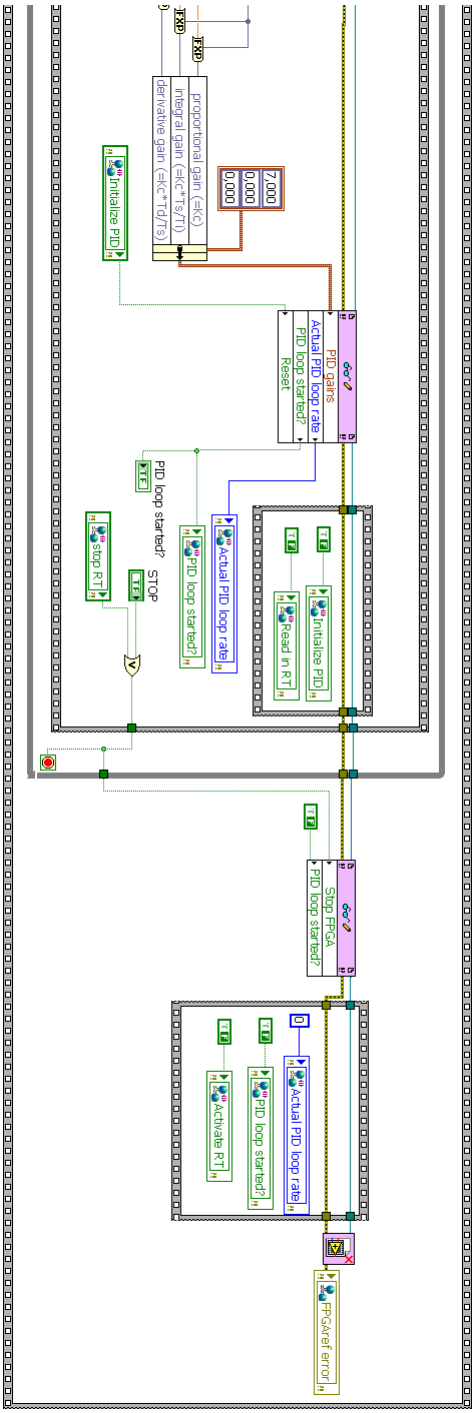

APPENDIX V:Host.vi block diagram, part 1

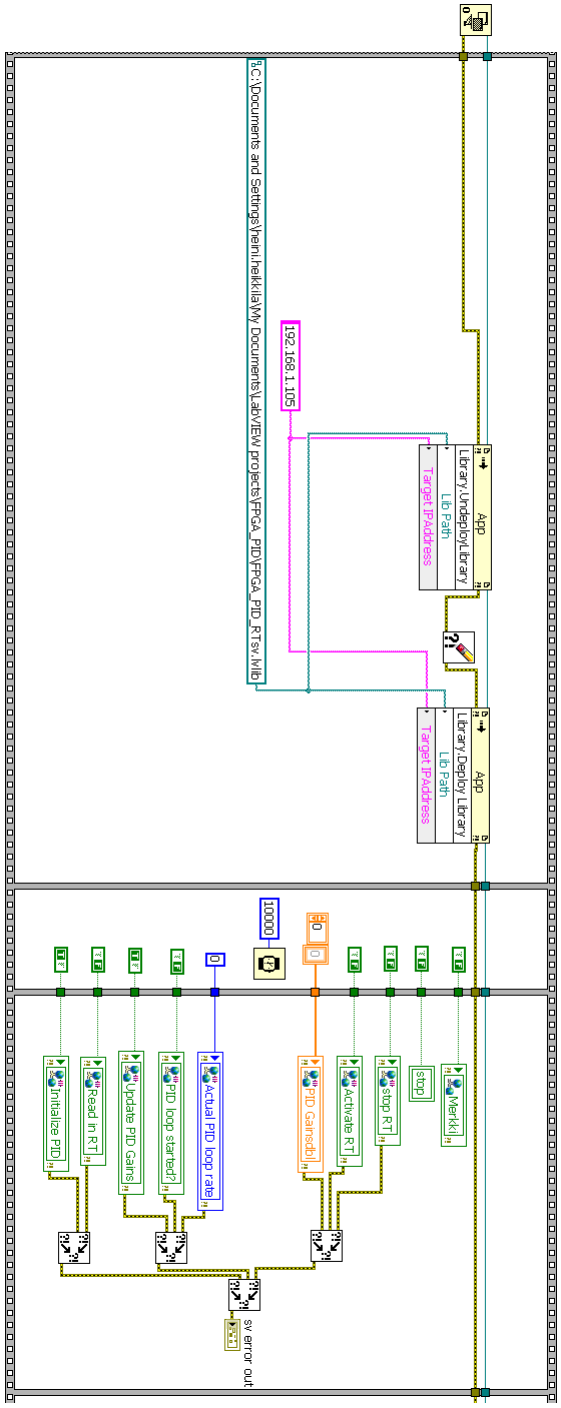

APPENDIX VI: Host.vi block diagram, part 2

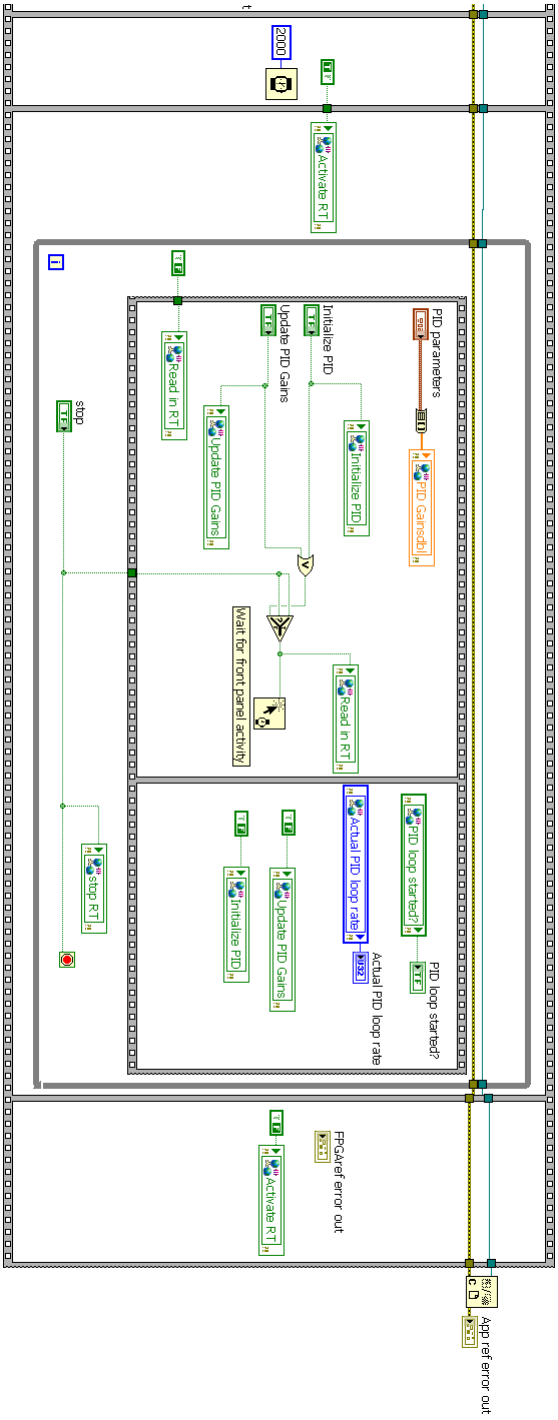

APPENDIX VII: Host.vi front panel